CONJUGATED POLYMERS WITH BENZOTHIADIAZOLE AND BENZOTRIAZOLE FOR ORGANIC SOLAR CELLS

A THESIS SUBMITTED TO
THE GRADUATE SCHOOL OF NATURAL AND APPLIED SCIENCES
OF
MIDDLE EAST TECHNICAL UNIVERSITY

BY

MERT CAN ERER

IN PARTIAL FULFILLMENT OF THE REQUIREMENTS
FOR
THE DEGREE OF MASTER OF SCIENCE
IN
CHEMISTRY

SEPTEMBER 2019

Approval of the thesis:

CONJUGATED POLYMERS WITH BENZOTHIADIAZOLE AND BENZOTRIAZOLE FOR ORGANIC SOLAR CELLS

submitted by **MERT CAN ERER** in partial fulfillment of the requirements for the degree of **Master of Science in Chemistry Department, Middle East Technical University** by,

Prof. Dr. Halil Kalıpçılar
Dean, Graduate School of **Natural and Applied Sciences** _____

Prof. Dr. Cihangir Tanyeli
Head of Department, **Chemistry** _____

Prof. Dr. Ali Çırpan
Supervisor, **Chemistry, METU** _____

Prof. Dr. Levent Toppare
Co-Supervisor, **Chemistry, METU** _____

Examining Committee Members:

Prof. Dr. Yasemin Arslan Udum
Technical Sciences Vocational School, Gazi University _____

Prof. Dr. Ali Çırpan
Chemistry, METU _____

Prof. Dr. Levent Toppare
Chemistry, METU _____

Assoc. Prof. Dr. Görkem Günbaş
Chemistry, METU _____

Assoc. Prof. Dr. Emren Nalbant Esentürk
Chemistry, METU _____

Date: 05.09.2019

I hereby declare that all information in this document has been obtained and presented in accordance with academic rules and ethical conduct. I also declare that, as required by these rules and conduct, I have fully cited and referenced all material and results that are not original to this work.

Name, Surname: Mert Can Erer

Signature:

ABSTRACT

CONJUGATED POLYMERS WITH BENZOTHIADIAZOLE AND BENZOTRIAZOLE FOR ORGANIC SOLAR CELLS

Erer, Mert Can
Master of Science, Chemistry
Supervisor: Prof. Dr. Ali Çırpan
Co-Supervisor: Prof. Dr. Levent Toppare

September 2019, 68 pages

In this study two novel random polymers, comprising benzothiadiazole and benzotriazole as the accepting units and benzodithiophene as the donor unit, were examined in terms of their photovoltaic performance. Moreover, effects thiophene and selenophene π bridges on optical, electrochemical and optoelectronic properties of the polymers were investigated. Optical band gap values of selenophene bearing P1 and thiophene P2 were found as 1.63 eV and 1.73 eV, respectively. Characterization of polymers via UV-Vis-NIR spectroscopy, cyclic voltammetry (CV), gel permeation chromatography (GPC) and thermal analysis were carried out. Organic solar cells (OSCs) were constructed and characterized in N_2 filled glove box. While the polymers act as electron donors, $PC_{71}BM$ was the electron acceptor in OSCs with the device structure of ITO/PEDOT:PSS/Polymer:$PC_{71}BM$/LiF/Al. As a consequence of measurements under standard AM 1.5 G illumination (100 mW/cm^2), the highest power conversion efficiency values were recorded as 1.60% and 3.83 % for P1 and P2 based OSCs, respectively.

Keywords: Organic Solar Cells, Selenophene, Thiophene, Benzothiadiazole, Benzotriazole

ÖZ

ORGANİK GÜNEŞ PİLİ UYGULAMALARI İÇİN BENZOTİADİAZOL VE BENZOTRİAZOL İÇEREN KONJÜGE POLİMERLER

Erer, Mert Can
Yüksek Lisans, Kimya
Tez Danışmanı: Prof. Dr. Ali Çırpan
Ortak Tez Danışmanı: Prof. Dr. Levent Toppare

Eylül 2019, 68 sayfa

Bu çalışmada, akseptör grup olarak benzotiyadiazol ve benzotriazol, donör grup olarak ise benzoditiyofen içeren iki özgün polimerin fotovoltaik performansları incelenmiştir. Buna ek olarak, tiyofen ve selenofen π köprülerinin, polimerlerin optik, elektrokimyasal ve optoelektronik özelliklerine etkileri çalışılmıştır. Selenofen içeren P1 ve tiyofen içeren P2 için optik bant aralığı değerleri sırasıyla 1.63 eV ve 1.73 eV olarak bulunmuştur. Polimerler, UV-VIS-NIR spektroskopisi, dönüşümlü voltammetri (CV),jel geçirgenlik kromatografisi (GPC) ve termal analiz gibi yöntemlerle karakterize edilmiştir. Organik güneş gözeleri, N_2 ile doldurulmuş eldivenli kabin sisteminde oluşturulmuş ve karakterize edilmiştir. Göze yapımında ITO/PEDOT:PSS/Polimer:$PC_{71}BM$/LiF/Al şeklinde düz cihaz mimarisi kullanılmış olup, polimerler elektron donörü, $PC_{71}BM$ ise elektron akseptörü olarak kullanılmıştır. Standard AM 1.5 G ışıması (100 mW/cm^2) ölçümler sonucunda, P1 ve P2 bazlı organik güneş gözeleri için maksimum güç dönüşüm verimi değerleri sırasıyla %1.60 ve %3.83 olarak kayıtlara geçmiştir.

Anahtar Kelimeler: Organik Güneş Gözeleri, Selenofen, Tiyofen, Benzotiyadiazol, Benzotriazol

To my beloved family…

ACKNOWLEDGEMENTS

I would like to declare my special thanks to my supervisor Prof. Dr. Ali Çırpan for giving me the opportunity of working under his supervision, on the topic of Solar Energy, which has become a huge motivation for my ongoing academic career. I also would like to thank to my co-advisor Prof. Dr. Levent Toppare, for his precious support throughout my work. I also would like declare that I am grateful for the efforts of Duygu Keleş and Şevki Can Cevher, on the syntheses of the polymers that have been characterized for this work.

I would like to acknowledge Dr. Gönül Hızalan Özsoy, for everything that I have learned on topic that I am concluding my Master's degree, both in terms of theoretical and practical knowledge.

I would also like to thank my labmates, Eda Bolayır and Eda Alemdar for their endless support and friendship throughout my studies, which have made everything look and go on much easier that it has to be for me.

I would also like to declare my highest gratitudes to my loveliest friends here in this department, Ece Ayça Yücel, Gülten Özkul and Meriç Çalışkan, who have experienced my happiest and most tense moments throughout my time here. The support they have given have become the biggest relief that I have achieved, for the moments that I felt like everything is about to collapse.

Consequently, I would like to thank my beloved family, who I have dedicated this thesis for. They are the ones who have made me the person I have become now. I owe everything that I have succeeded up to now, to them.

This study supported by the Scientific and Technological Research Council of Turkey (TUBITAK) (Project number: 115M036). I would also like to thank to METU Central Laboratory, for GPC, TGA and TEM analysis.

TABLE OF CONTENTS

LIST OF TABLES

TABLES

LIST OF FIGURES

FIGURES

LIST OF ABBREVIATIONS

ABBREVIATIONS

ACN	Acetonitrile
Ag	Silver
Al	Aluminum
AM1.5G	Air mass 1.5 global
BHJ	Bulk heterojunction
c	Speed of light
C_{60}	Fullerene
Ca	Calcium
CB	Chlorobenzene
$CHCl_3$	Chloroform
CN	Chloronaphthalene
CV	Cyclic voltammetry
D-A	Donor-acceptor
DIO	1,8-diiodooctane
DPE	Diphenylether
DSC	Differential scanning calorimetry
E_b	Exciton binding energy
E_g	Band gap
E_g^{el}	Electronic band gap
E_g^{op}	Optical band gap
$E_{HOMO,D}$	Highest occupied molecular orbital of the donor molecule
$E_{LUMO,A}$	Lowest unoccupied molecular orbital of the acceptor molecule
$E_{n\text{-}doping}$	Reduction potential
E_{ox}^{onset}	Oxidation onset potential
$E_{p\text{-}doping}$	Oxidation potential

E_{red}^{onset}	Reduction onset potential
ETL	Electron transport layer
Fc/Fc^{+}	Ferrocene/ferrocenium
FF	Fill factor
FTO	Fluorine-doped tin oxide
GPC	Gel permeation chromatography
h	Planck's constant
HOMO	Highest occupied molecular orbital
HTL	Hole transport layer
ICT	Intramolecular charge transfer
ITO	Indium tin oxide
J_{max}	Current density value correlated to P_{max}
J_{SC}	Short circuit current density
J-V	Current density-voltage
LED	Light emitting diode
LiF	Lithium fluoride
LUMO	Lowest unoccupied molecular orbital
M_W	Weight average molecular weight
M_w	Molecular weight
NIR	Near infrared
O_2	Oxygen gas
o-DCB	1,2-dichlorobenzene
OFET	Organic field-effect transistor
OLED	Organic light emitting diode
OSC	Organic solar cell
$PC_{61}BM$	Phenyl-C61-butyric acid methyl ester
$PC_{71}BM$	Phenyl-C71-butyric acid methyl ester
PCE	Power conversion efficiency
PEDOT:PSS	Poly(3,4-ethylenedioxythiophene)-polystyrenesulfonate
PES	Polyethersulfone

P_{max}	Maximum power generated
PSC	Polymer solar cell
Pt	Platinum
$TBAPF_6$	Tetrabutylammonium hexafluorophosphate
TEM	Transmission electron microscopy
TGA	Thermogravimetric analysis
UV-Vis	Ultraviolet-visible
v/v%	Volume ratio
V_{max}	Voltage value correlated to P_{max}
V_{OC}	Open circuit voltage
w/v%	Weight per volumee percent
w/w	Weight ratio
λ_{max}	Maximum absoprtion wavelength
λ_{max}^{onset}	Onset absorption wavelength
η	Power conversion efficiency

CHAPTER 1

INTRODUCTION

1.1. Solar Energy

1.1.1. Interest on Solar Energy

Energy production has become a very critical problem due to increasing human population and decreasing fossil fuel resources [1]. In today's society, increasing human population and enhancing effects of global warming are considered among the most important problems. Excessive use of fossil fuels enhances the carbon dioxide emission to the atmosphere, which is a contributing factor for the climate change [2]. As a result, there have been a search for renewable and clean energy for the last decades. Among these, the most feasible source to be used is the solar energy, due to the increasing intensity of solar radiation reaching the earth during recently, and inevitable existence of sunlight during specific periods of the day [3,4].

1.1.2. Solar Technology

The solar technology is mainly based on the use of the semiconducting materials. In the market, the conducting systems are commonly based on inorganic materials. The solar materials are mainly consisted of silicon based inorganic materials. These materials possess several advantages such as high conductivity, charge mobility and low binding energy for excitons which all yield the relatively higher power conversion efficiency (PCE) values with an average of 20% [5–7]. In addition, enhanced stability towards air and light of the silicon materials are appealing characteristics of them to be the most convenient candidates among other materials to be used for solar cells. However, disadvantages such as expensive and challenging production methods, heavy weight, low absorption coefficients towards solar irradiation and non-tunable energy level characteristics necessitate the search for

alternative materials in this sphere of research [8,9]. There are several new technologies that are mostly under research and development stage, such as hybrid, tandem, dye-sensitized, perovskite and organic solar cells. All of these technologies are based on new materials, to create solar systems that contain the properties that the silicon based systems are lacking.

1.2. Conjugated Polymers

Conjugated polymers aroused interest for the systems that require semiconducting materials, due some of their promising properties. The semiconducting property of these materials arises from the conjugated structure they possess.

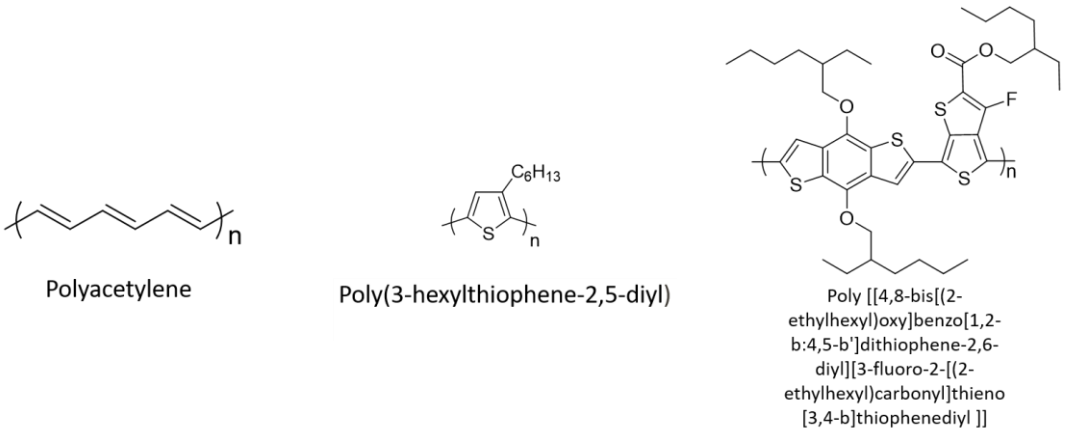

Figure 1.1. Examples for the structures of some common conjugated polymers

In Figure 1.1., some commonly used conjugated polymers are illustrated as an example. The sp^2-hybridized carbon based polymer structure provide electron delocalization throughout the polymer backbone. This results in the high electron polarizability and the semiconducting properties of the polymers [10]. For this reason, conjugated polymers are also called as conductive polymers. The work on the discovery and the development of the conjugated polymers rewarded Alan J. Heeger, Alan G. Mcdiarmid and Hidaki Shirakawa the Nobel Prize in Chemistry, in

2000. The work was mainly based on the enhanced conductivity of a conjugated polymer, polyacetylene, upon treatment with iodine vapor (I_2) [11].

$$3x/2I_2 + (CH)_n \rightarrow (CH)_n^{x+} + xI^-_3$$

Upon oxidation with halogen treatment, a hole and electron vacancy on the backbone is generated. As previously mentioned, this vacancy is carried through the polymer backbone bearing alternating single and double bonds. The process is called doping and it enhances the conductivity of polyacetylene up to 38 Scm^{-1}, which is the maximum value observed for polyacetylene.

After the discovery of conductive polymers, there have been an extensive research on the development and applications of the conjugated polymers. The advantages of such materials such as low cost, low weight, solution processability, simple device fabrication and tunability of the chemical structure and characteristics [10,12]. The possibility of synthesizing several conjugated polymers with different structures containing distinct monomer groups, encourage most researchers to focus on synthesizing novel molecules with promising characteristics as semiconducting materials.

1.2.1. Application Areas of Conjugated Polymers

Due to the semiconducting properties and the advantages of the conjugated polymers compared to their silicon counterparts, these molecules are promising candidates in terms of some application areas of materials science. These materials can be used in organic field-effect transistors (OFETs), electrochromic devices, organic light emitting diodes (OLEDs) and organic solar cells (OSCs) [13].

1.2.1.1. Electrochromic Devices

Electrochromism is basically defined as the reversible colour change of a material upon applied potential or an electric current. The process undergoes with the principle based on oxidation-reduction reactions. As a result of oxidation reduction processes taking place, there is a change in optical properties occur for the material

being used. This is due to the formation of new absorption bands, as a response to the electrochemical stimulus. Electrochromic devices can both be organic or inorganic based. Among these, conducting polymers possess superiorities as electrochromic materials, such as long-term stability, short switching time values which could be altered via synthetic methods, high coloration efficiency, enhanced optical contrast, extensive optical memory and multicolour properties due to commutable band gap values of organic molecules [14].

The working principle is mainly based on the formation of polarons due to applied potential. Polarons are basically the positive charge carrying radicals, which are formed due to the oxidation of conjugated polymers, in other words, when they are p-doped, in which an electron is removed from its valence band, stimulated by the potential applied. Further oxidation forms the bipolarons which are dications that carry two positive charges on them. This results in the formation in an additional absorption band in the absorption spectra of the polymer, between 700-1000 nm. The formation of these charge carriers can also be observed from the depletion of the absorption band of the neutral conjugated system, which corresponds to the π-π^* transitions. The reason for obtaining the polaron band at a relatively high band gap is the formation of additional energy states between the highest occupied molecular orbital (HOMO) and the lowest unoccupied molecular orbital (LUMO) of the conjugated molecule, formed upon oxidation, as illustrated in Figure 1.2b [15,16].

The efficiency of an electrochromic device is defined by some parameters which were mentioned previously.

- *Electrochromic Contrast* is the change in percent transmittance as the polymer achieve its highest optical contrast at a specific wavelength.
- *Coloration Efficiency* is the amount of charge required for a material to experience a colour change.
- *Optical Memory* is basically defined as the time that the electrochromic device sustains a specific colour

- *Switching Time* is the time required for the device to switch from one colour to another
- *Device Stability* is the parameter that defines the time that the device could function without degrading. As the applied voltage increases, the device lifetime decreases.

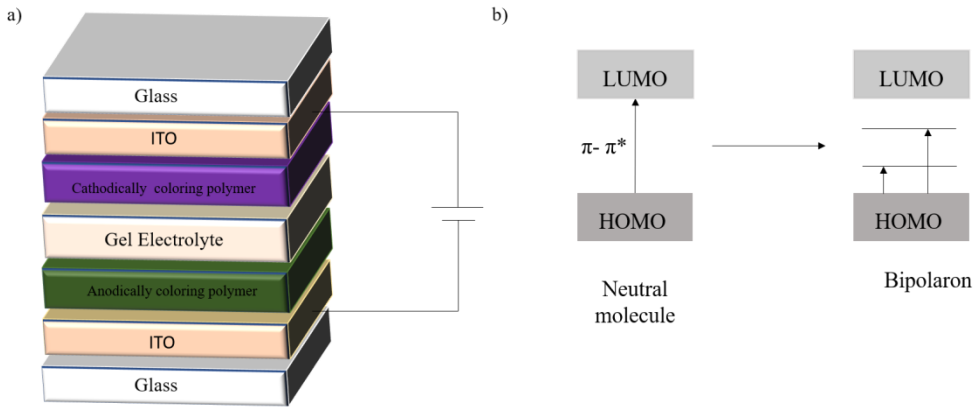

Figure 1.2. a) Schematic representation of an electrochromic device, b) illustration of formation of new energy states with oxidation of conjugated polymers

The device architecture for an electrochromic device is depicted in figure 1.2a, in which both the anodically and cathodically coloring polymers are sandwiched between two indium tin oxide (ITO) electrodes. In the system, ITO substrates function as the working electrodes, and the gel electrolyte is used to provide ionic conductivity between the polymer and the sandwiched architecture. The potential difference is applied between two electrodes, for the polymers to perform a color change [17].

Two most common application areas of the electrochromic devices are the rear-view mirrors and smart windows.

1.2.1.2. Organic Light Emitting Diodes (OLEDs)

Organic light emitting diodes, (OLEDs) are the devices that emit light upon applied potential, and contain conjugated organic materials present as a thin film. OLED

technology aroused interest mainly for the display technologies. Owing to the superiorities that the conjugated materials possess compared to their inorganic counterparts that were mentioned previously, forced the researchers to concentrate on the OLEDs as an alternative to LEDs.

The idea of using organic materials for the LED applications was mainly inspired by the work that Andre Bernanos performed on the organic material “acridine orange”, which proved that the electroluminescence can be achieved on conjugated organic systems, in 1953. This was followed by the work of Pope et al. at 1965, which proved that anthracene can perform luminescence [18]. Thus, the milestone for the applications of OLED technologies took place in 1987, when Ching. W. Tang and Stephan V. Slyke achieved bright luminance from a device comprising Alq3 (tris(8-quinolinolato)-aluminium(III)), sandwiched between two electrodes [19]. The use of conjugated polymers for this technology was first performed by Richard Friend, with the construction and characterization of the single layer OLED by the use of poly(p-phenylene vinylene) (PPV) as the emissive layer, which exhibits enhanced fluorescence when operated [20].

The working principle of OLEDs can be summarized in three main steps.

- Charge injection on the corresponding electrodes due to the applied potential difference
- Transportation of the injected charges to the emissive layer, which is a conjugated organic molecule, and collection of the electrons at the LUMO, and the holes at the HOMO
- Radiative recombination of the electrons and the holes at the HOMO, results in emission of light

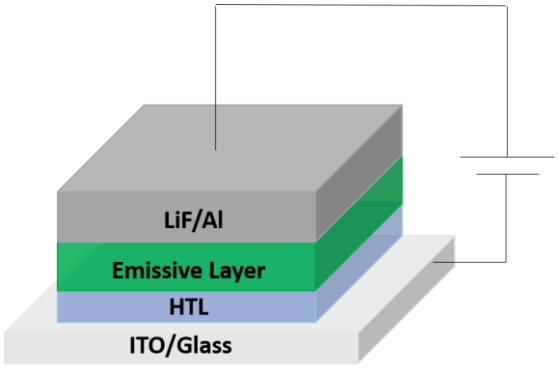

Figure 1.3. Schematic representation of basic OLED devices

As it can be seen from Figure 1.3, the emissive layer is sandwiched between two electrodes. The ITO coated glass substrate functions as anode for the conventional architecture given, where holes are injected. Top contact that contains lithium fluoride (LiF) and aluminum (Al) functions as the cathode, in which the electrons are injected. The holes reach the emissive layer with the help of the hole transport layer (HTL), which eases the transportation of holes, by reducing the energy barrier between the anode and the emissive layer. The emission is transmitted by the transparent ITO coated glass substrate.

1.3. Organic Photovoltaics

As mentioned in section 1.1, the extinction of fossil fuels and the growing effects of global warming has urged the search for clean and renewable energy sources. Among them, the solar energy is the most convenient. Generally, in the market crystalline silicon based inorganic materials are used for the construction of solar cells, reaching the power conversion efficiency of 15-20%. However, as mentioned previously, some characteristics of the conjugated organic molecules, the focus of the scientific research shifted to organic photovoltaics. As the name recalls, photovoltaics are the systems that convert sunlight into electrical energy. Organic photovoltaics are the photovoltaic systems that are established by using semiconducting organic molecules. As it was stated before, semiconducting

molecules are conjugated polymers or small molecules. Due to their low cost, simple fabrication to large scale, solution processability, flexibility and low weight, organic photovoltaics aroused interest recently. Therefore, extensive researches have been executed on this specific topic during last decades [10].

The most basic form of the organic photovoltaics is the organic solar cells (OSCs). These devices are basically diode systems that generate current as a result of collection of the charges generated as a result of absorption of sunlight. For the organic solar cells, the absorbing materials are the conjugated organic molecules. The first successful construction of an organic solar cell was performed by C. W. Tang in 1986, proposing a bilayer structure for the first time, different from the former single layer devices [21]. Power conversion efficiency was recorded as 1% for this work. The use of two distinct layers was designed for more effective charge separation, due to the device contained p-type copper phthalocyanine (CuPc) vacuum deposited on ITO to hold the holes, which are basically the positive charges formed due to excitation of the electron. Onto the p-type material, n-type perylene tetracarboxylic derivative was deposited to attain the electrons. The cathode was a thin silver (Ag) layer vacuum evaporated onto the n-type material. The appropriate use of p-type and n-type materials are important for efficient operation of organic solar cells, and the functions of these materials will be discussed in more detail in the following sections of this thesis.

With all the research and development efforts put on the improvement of the organic solar cell technologies, today, the power conversion efficiency values achieved with the aid of this concept have overcome the level of 17% [22]. To reach this level, some problems occur with the use of organic photovoltaic systems have been aimed to be solved. To have a better insight about these problems and the milestones that lead the organic solar cells to today's technology, the device architecture and the working principle should be well understood.

1.3.1. Device Architecture and Working Principle of Organic Solar Cells

The working principle of organic solar cells can be summarized in four main steps [23].

- Absorption of light by the conjugated molecule and the formation of bound electron hole pairs, so called excitons
- Exciton diffusion to the donor acceptor interphase, where the charge separation occurs
- Charge separation at the donor acceptor interphase
- Collection of the charges at the corresponding electrodes

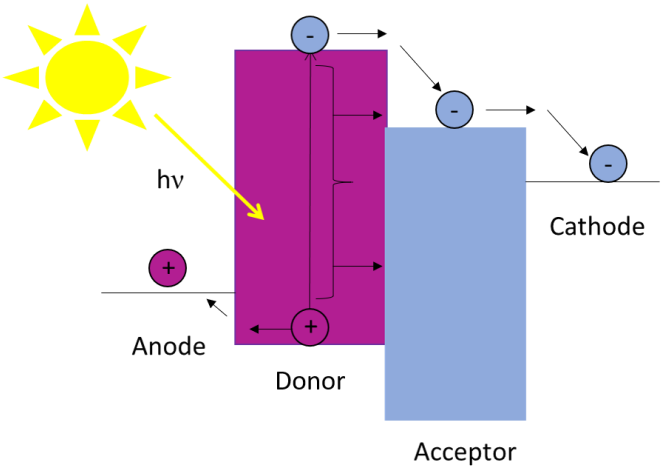

Figure 1.4. Illustration of working principle of organic solar cells

As can be depicted from figure 1.4., organic solar cells require both donor and acceptor molecules to function properly. Terms donor and acceptor stand for electron donor and electron acceptor molecules. Conjugated polymers that are designed to absorb the sun light to execute the first step of the working principle, function as the electron donors, and they are classified as p-type materials. When the light is absorbed and the electron is excited to a higher energy level, the hole and the electron are in coulombic interaction until the charge separation occurs. Thus, an

exciton is defined as the bound electron hole pair [10,24]. The system requires a p-n junction to attain the effective exciton dissociation and charge separation process, hence an n-type electron accepting molecule is required. The reason for this is the high exciton binding energy (E_b) that the conjugated organic molecules possess compared to inorganic materials [25]. The value of this parameter is generally recorded as greater than 1 eV for the conjugated organic molecules [26], while the value is generally accepted as 14.7 meV for silicon based inorganic materials [27]. This is correlated to the use of an n-type material for the construction of an organic solar cells, as conjugated molecules cannot undergo a charge separation at room temperature, without an acceptor molecule acting as a driving force for the process, with high electron affinity. This idea was first come up when the ultrafast charge transfer from a conjugated polymer to fullerene by Heeger and Sariciftci was performed in 1992 [28]. This work also influenced the use of fullerene derivatives as p-type molecules. Silicon based technologies do not require p-n junction to process, as the exciton binding energy is low enough for the material to perform dissociation at lower temperatures.

Another factor that is effective for the efficient operation of an organic photovoltaic system, is the energy barriers that the charges pass through to reach the electrodes. For the electrodes, the work function values are important. Work function of a metal is defined as the minimum amount of work required to remove an electron from the metal. As the holes are accumulated at the anode, work function of it should be relatively high, so that the holes could reach the low-lying Fermi level of the anode from the HOMO of the donor molecule, as illustrated in Figure 1.4. The work function of the cathode layer should be relatively lower as the electronegativity of it is sufficiently high to contain electrons. The LUMO level of the acceptor molecule should also be relatively low, so that it could bear stable excited states and be able to hold the electrons when the exciton is dissociated [10].

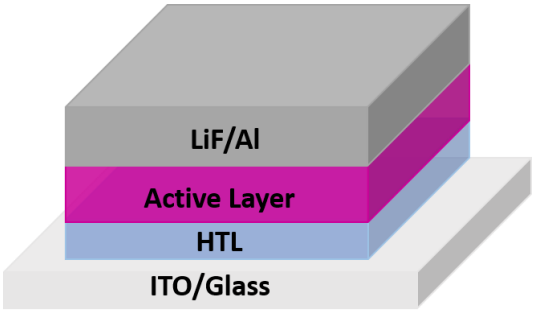

Figure 1.5. Schematic representation of a conventional organic solar cell

As can be seen from figure 1.5., from bottom to top, a sample organic solar cell contain an transparent ITO coated glass substrate which serves as the anode and transmits the incoming solar radiation to reach the active layer, a hole transport layer (HTL) coated onto it, active layer containing donor and acceptor molecules, an active layer sandwiched between two electrodes and a LiF/Al metal layer as the top contact functioning as the cathode. The designs, the methods of processing and the importance of all the layers included will be explained in more detail in the following sections of this thesis.

1.3.1.1. Active Layer and Bulk Heterojunction Principle

As mentioned previously, active layer is where the absorption of the incoming solar irradiation and all the other steps stated up to the collection of charges at the corresponding electrodes. Extensive absorption coefficient values of conjugated polymers are the main reason of using them as the active materials for the organic solar cells. Organic solar cells that are constructed with the use of conjugated polymers are also called polymer solar cells (PSCs). n-type molecules are also included inside the active layer for enhanced exciton dissociation. Diffusion of the excitons to the donor acceptor interphase is required for the charge separation to occur. For this manner, bilayer devices, in which the p-type and n-type materials are deposited as two distinct layers, as it was performed for the wok of C.W. Tang, were designed and established for efficient energy conversion [21]. However, with this

method, performance of the OSCs did not reach the desired level, due to the low diffusion length values that the conjugated polymers possess. Diffusion length is the parameter that defines the distance that an exciton can travel without experiencing any recombination. The values are usually less than 20 nm, which means that for a bilayer device, number of excitons performing recombination before reaching the interphase is significantly high which reduces the overall efficiency of the OSC [29].

Bulk heterojunction (BHJ) idea was developed by N. S. Sariciftci and A. J. Heeger to overcome the problems arising from the low diffusion length of the conjugated polymers [23]. The system is mainly formed by mixing the donor and acceptor molecules in the same blend. The design reduced the distance for the excitons to reach donor interphase, by increasing the donor acceptor interfacial area. These lead the improvement of the exciton dissociation and overall power conversion efficiency values for the OSCs. Hence, the application of BHJ concept started a new era in terms of the development of OSCs [30].

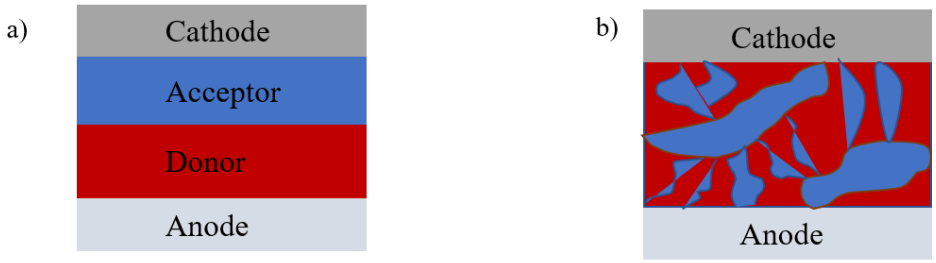

Figure 1.6. Schematic representation of a) bilayer OSC b) BHJ OSC

Figure 1.6. illustrates the difference between the bilayer and BHJ layers. As can be seen from Figure 1.6.b, bulk heterojunction provides an interpenetrating network between the donor and the acceptor molecules to enhance the number of charge separation taking place. The bicontinuous network in the active layer is illustrated in figure 1.6.b, as an example of an ideal morphology. The paths reaching the electrodes are called the percolation pathways and required for the charges to reach the corresponding electrodes, without being trapped and recombine [31,32].

1.3.1.1.1. Donor and Acceptor Molecules

1.3.1.1.1.1. Characteristics of Ideal Donor Molecules

Apart from being conjugated systems, donor molecules should possess some other characteristics to serve efficiently as a donor molecule. The structures of the conjugated polymers can be altered by synthetic methods to achieve the desired properties. One of the characteristics that the semiconducting polymers should attain is the high charge mobility to perform efficient charge transport towards the anode. Well-organized planar backbone, little variation in torsion angle, enhanced regioregularity and high order crystallinity are the factors that enhance the charge mobility [33]. The conjugated polymers to be used for OSC applications are usually synthesized as donor-acceptor (D-A) type, where the electron rich monomers which serves as the donor, and the electron poor acceptor units are coupled [34]. The monomers contain alkyl side chains, for optimized solubility [35]. Recently, conjugated polymers are being synthesized with antisymmetric alkyl side chains. This improves the order of crystallinity and the charge mobility for the polymers [36].

The band gap (E_g) of the synthesized conjugated polymer is also very important in terms of its photovoltaic performance. E_g of a conjugated polymer is basically defined as the energy gap between its HOMO and LUMO levels. E_g values should be optimized to keep the parameters that contribute to the power conversion efficiency of the device constructed. The portion of the solar spectrum that the polymer absorbs is directly related to the photocurrent generated by the device. Standard solar spectrum that is used for the characterization of the OSCs is AM1.5G, which will be discussed in more detail in the following sections, covers a spectrum from 300 to 1000 nm. That means a significant portion of the spectrum resides on the near infrared (NIR) region. So that low band gap values are preffered, ideally around 1.2 eV, to absorb in the NIR region [37,38]. D-A polymer synthesis idea mainly came up for the need of tailoring the band gap of the polymers. Donor

moieties in the polymer backbone are mainly units that possess high energy frontier orbitals as they are electron rich. Electron poor acceptor moieties exhibits lower energy frontier orbitals. Coupling of these two groups results in the hybridization of the frontier orbitals, resulting a polymer HOMO level closer to the HOMO of the donor unit, and a LUMO level closer to the energy levels of the acceptor moiety. This results in narrow band gap formation [39].

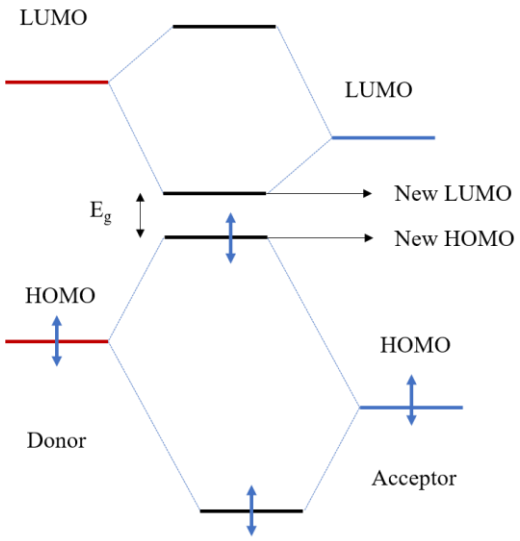

Figure 1.7. Molecular orbital hybridization for a D-A type conjugated polymer

However, lowering the E_g values below the ideal values might result in reduction of open circuit voltage (V_{OC}) which decreases the power conversion efficiency. Therefore, E_g values should be optimized. The concept of V_{OC} will be discussed in more detail in the following sections.

Molecular weight (M_w) of the polymer is also critical for the performance of the OSC. Low M_w causes lower absorption of the polymers towards the solar spectrum and excessive solubility leading wider fibrils of polymers reducing the efficiency of exciton diffusion to the donor acceptor interphase without charge recombination [40]. On the other hand, when M_w is too high, solubility of the polymers in the

organic solvents decrease, resulting in problems of processing and a decrease in photovoltaic performance.

Recently, synthetic variations on conjugated polymers to reduce E_B and increase the diffusion length values are being studied and successful efforts have been put to increase the efficiency of the OSCs. Incorporation of π-bridges to enhance the π-conjugation length, fluorination of the backbone to manipulate the frontier orbital energy levels are some of the synthetic variations being applied, and most of the attempts improved the results.

1.3.1.1.1.2. Acceptor Molecules

Generally, fullerene (C_{60}) based molecules are used as the acceptor groups for BHJ based OSCs, due to the triply degenerate, stable excited states they possess and advanced electron transport properties [41]. However, chemically modified versions of the fullerene derivatives are used, such as phenyl-C61-butyric acid methyl ester ($PC_{61}BM$), with enhanced solubility in organic solvents compared to unmodified fullerene. The solubility is enhanced with the incorporation of a side chain to the fullerene structure [42]. $PC_{71}BM$, the C_{70} derivative is more commonly used compared to $PC_{61}BM$ as acceptor molecule, due to higher absorptivity coefficient it possesses and higher potential to form self-organized and ordered phase separation and morphology with the conjugated polymers [43]. It is because of the loss of symmetry for the Buckyball in case of C_{70}. Processing PCBM derivatives as acceptor molecules for the BHJ might be limiting in terms of the power conversion efficiency of OSCs, as the energy levels cannot be altered, they can attain limited interaction with the conjugated polymers in the BHJ film, and they possess low absorptivity coefficients towards the solar spectrum. Hence, recently, there have been excessive efforts on synthesizing non-fullerene acceptors, which are designed to comprise the characteristics that the fullerene derivatives are lacking, and the superiorities of PCBM as an acceptor at the same time. In this manner, non-fullerene

acceptors, such as ITIC and IEIC are being used to improve the performance of organic photovoltaic devices [44].

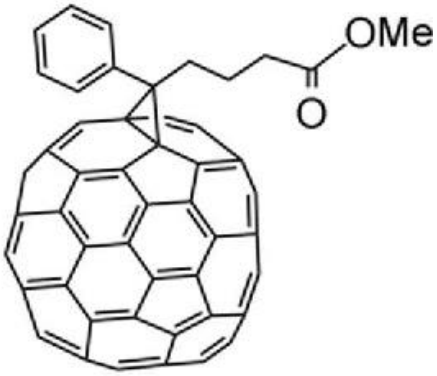

Figure 1.8. Structure of $PC_{71}BM$

1.3.1.1.2. Active Layer Morphology

The morphology of the active layer is a key contributor for the overall efficiency of an OSC. Even though the BHJ concept solves the problem of exciton dissociation, if the active layer morphology does not exhibit percolations that eases the transportation of the charges to the electrodes. For such a situation, charges might get trapped and non-geminate recombination might occur. Note that geminate recombination is the recombination taking place before any dissociation occur, and the non-geminate recombination is the recombination after the charge separation process [45].

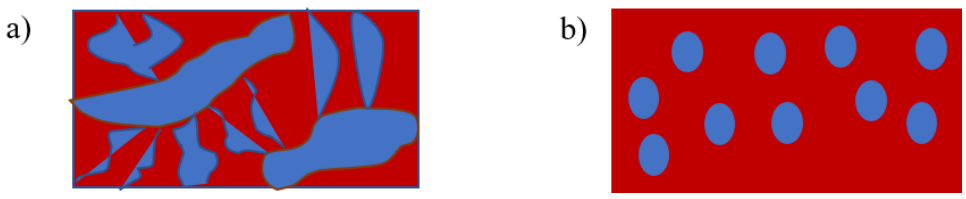

Figure 1.9. Schematic representation of a) ideal morphology b) non-ideal morphology for a donor acceptor blend, where the red region stands for the donor and blue region stands for the acceptor

Figure 1.9. illustrates the difference between an ideal and a morphology with a poor quality. As mentioned before, the main difference is the percolations that leads the charges to the corresponding electrodes. Due to the problems that a poor morphology could cause, morphology control at the nanoscale is important for efficient OSC operation [46].

1.3.1.1.2.1. Morphology Control

1.3.1.1.2.1.1. Donor-Acceptor (D-A) Blend Ratio

Donor-acceptor blend ratio means the relative ratio of the quantity of donor inside the active layer blend to the amount of acceptor molecules. Both contribute to the overall performance of the OSC differently. The donor molecule mainly functions as the absorber so that increasing the quantity of the donor molecule mainly results in the enhancement of the absorption of the incoming solar irradiation by the active layer. The acceptor is mainly responsible for the charge transport properties of the active layer. As the ultrafast charge transfer is achieved at the donor acceptor interface, theoretically, an increase in the charge separation efficiency and the transportation of the separated charges to the corresponding electrodes is observed. So that the absorbance and the charge transport should be balanced in the active layer morphology, by optimizing the D-A blend ratio [47,48].

1.3.1.1.2.1.2. Choice of Solvent

Solvent processability of the conjugated polymers is one of the most important advantages for the OSC applications. Hence, choice of solvent is important to obtain a good morphology of the active layer. Usually, D-A blend films processed from high boiling point solvents, such as chlorobenzene (CB) or orthodichlorobenzene (o-DCB), reaching the values around 180°C, possess higher performance, compared to low boiling point solvents such as chloroform. The main reason for this is that the blend can perform thermal treatment at higher temperatures, so that there is more time for the donor molecules to crystallize and align more regularly. For chloroform, as the solvent evaporates rapidly, an acceptor rich morphology in a polymer rich

matrix is formed, in which the domains with large size form. Large domain size yields less interfacial area, which reduces the number of efficient charge separation. This situation causes the exciton dissociation without charge recombination and charge transport charge transport to become more challenging. However, some polymers possess insufficient solubility in high boiling point solvents, such as CB and o-DCB, so that alternative solvent systems such as chloroform might be required. To achieve tolerable solubility and better morphology at the same time, with smaller domain size and more interpenetrated D-A network, co-solvent systems are also used. In such systems, chloroform acts as the host solvent, different volumes of o-DCB up to 5% vol is added to the solvent system, to achieve optimum morphology. Figure 1.10. illustrates the change in morphology as D-A blends are processed from different solvents [49,50].

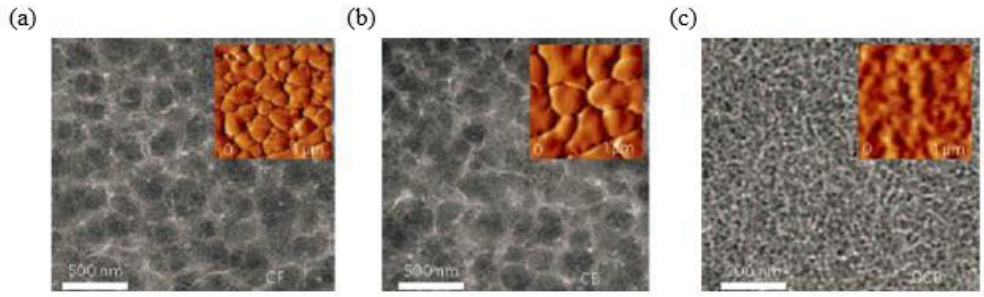

Figure 1.10. TEM images of thin films spin cast from (a) CF, (b) CB, and (c) DCB

1.3.1.1.2.1.3. Thermal Annealing

The D-A phase separation takes place in the solution. However, as the active layer is spin-casted, the process is paused. The phase separation and the alignment of the D-A blend can be further improved by specific methods. Recent researches have proven that the thermal annealing of the film deposited at high temperatures up to 150°C improves the performance of the active layer and the OSC. This improvement is correlated to the enhanced crystallinity of the phase separated donor and acceptor networks, improving the charge mobility and transportation through the film,

enhancing the efficiency of separated charges to reach the corresponding electrodes. The increase in the efficiency of the OSCs upon thermal annealing is related to the decrease in series resistance. These improvements could be proven by the red-shift observed for the UV-Vis absorption spectroscopy of the polymers, due to enhancement of interchain interaction of highly organized polymers with improved crystallinity. For one of the most common conjugated polymers used in the OSC applications, poly(3-hexylthiophen-2,5-diyl), it is proven that to achieve a significant power conversion efficiency value, thermal annealing around 110°C is required, by several researches [51].

1.3.1.1.2.1.4. Solvent Annealing

Solvent annealing is another technique to improve the phase separation of the film. It is a slow growth process that alters the orientation of the polymer film. The ordering of the polymer can be controlled with the manipulation of the rate of solvent annealing. The process includes the solvent transmitting the mobility of the polymer, and sudden removal of defects at the film. This method results in highly oriented and nearly defect free formation of improved morphology, with interpenetrated D-A phase separation [52,53].

1.3.1.1.2.1.5. Processing Additive

Processing additive provides one of the most effective and basic methods to control the morphology of the active layer. Trace amounts of additives can serve as a useful tool to improve the morphology of the D-A blend. Additives generally display 3 specific characteristics.

- They should be miscible with the host solvent.
- They comprise higher boiling point compared to the host solvent.
- They exhibit selective solubility towards the acceptor molecules, such as the enhanced side chain solubility provided for PCBM.

When the D-A blend solution is cast, the phase separation might yield with the domain sizes that are too small or too large compared to the optimum scale. This causes problems with the exciton diffusion and charge transport and might increase the number of charge recombination. When the solution is processed via additives, the selectively dissolved PCBM molecule are interpenetrated through the polymer matrix, enhancing the D-A interfacial area and decreasing the domain size. Without additives, PCBM molecules aggregate by forming undesired phase separation with the donor type conjugated polymers. 1,8-Diiodooctane (DIO), chloronaphthalene (CN) and diphenyl ether (DPE) are common processing additives that increase the power conversion efficiency of the OSCs via improved morphology, by forming bicontinuous interpenetrating network between the donor and acceptor molecules. In addition, as the additives are less volatile compared to the host solvent, allowing to blend to perform the bicontinuous D-A interpenetrating network phase separation to take place before the solvent evaporates during thermal treatment of the solution. Figure 1.11. illustrates how acceptor molecules such as PCBM is dispersed through the polymer matrix to form the interpenetrating network, without aggregating, by processing with the solvent additives [54,55].

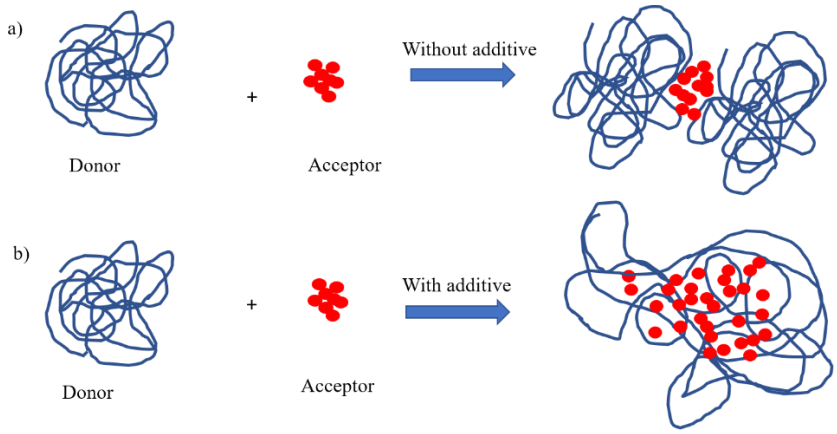

Figure 1.11. Illustration of the effect of additive treatment for the phase separation of D-A blends

1.3.1.1.2.1.6. Active Layer Thickness

Solution processable D-A blends are spin cast onto the HTL, to form a thin layer film. The rate of spin casting process is inversely related with the Thickness of the film is a key parameter for the photovoltaic performance of a conjugated polymer. Optimum thickness is a characteristic property for a specific D-A blend, depending on several parameters. As mentioned previously, photocurrent generated by the OSC is directly related to the portion of the solar spectrum absorbed by the active layer. Enhanced thickness results in increased absorption of the active layer towards solar irradiation. So for the polymers with relatively lower absorptivity coefficient values, thickness of the active layer should be high to harvest the sunlight efficiently. However, as discussed previously, organic conjugated polymers possess low diffusion length values. Compared to their silicon based inorganic counterparts, charge mobilities are proven to be lower. So that for polymers with low diffusion length and charge carrier mobility, excessive thickness might result in several recombination processes before the charges reach the electrodes from the active layer. Thus, active layer thickness should be optimized for improved morphology. Usually, for D-A blends containing conjugated polymers as the donor molecules, the optimum active layer thickness is determined to be 100 nm. However, this value could be higher or lower for specific polymers, due to its absorptivity and charge transport properties, as mentioned before [56].

1.3.1.1.2.1.7. D-A Blend Solution Concentration

Concentration of the D-A blend solution should also be optimized to achieve optimum morphology for a conjugated polymer being characterized. Again, similar to the case of achieving thicker active layers, increasing concentrations improves the absorption of the solar spectrum by the D-A blend. Yet, D-A blend solution concentrations exceeding 40 mg/mL are not usually included in the optimizations of the morphology or possess no improvement on the photovoltaic performance of the polymers. This is mainly caused by the solubility problems that the blend

experiences at very high concentrations. In addition, when the concentration is too high, again the thickness of the active layer processed might exceed the optimum values, reducing the efficiency of the photocurrent generation by the device and the overall photovoltaic performance of the polymer [57].

1.3.1.2. Anode

Indium tin oxide (ITO) and fluorine-doped tin oxide (FTO) are generally used as the anodes for OSCs. FTO is usually preferred when the device is processed at high temperatures, as its thermal stability is higher compared to ITO. The high work function, good conductivity, high transparency in the visible region and non-toxic nature of ITO make it a good candidate to be used as the anode. Work function of ITO is calculated to be around 4.70 eV, which enables the holes to reach the fermi level from the HOMO of the donor molecules. The transparency in the visible region is higher than 90%, which transmits the solar irradiation towards the active layer, for efficient absorption. Again, high conductivity values reaching 15 Ω/sq, eases the charge collection and the energy conversion performed by the device [58–60].

1.3.1.3. Hole Transport Layer (HTL)

Generally, for OSCs built with conventional architecture, between the anode and the active layer, there is HTL coated to reduce the energy barrier between those two layers. HTL should comprise specific aspects to serve as an OSC with high photovoltaic performance [61]:

- HTL requires semiconducting properties.
- It should possess high transmittance in the visible region.
- It should possess relatively high E_g value, low HOMO level to reduce the energy barrier with the HOMO of the donor polymer and high LUMO level to block possible electron transport from acceptor moieties.

In the earlier stages of development of OSCs, polyaniline was used as the HTL. However, recently, the most popular material used as the HTL for OSCs is the

polymeric material, named as poly(3,4-ethylenedioxythiophene)-poly(styrenesulfonate) (PEDOT:PSS). PEDOT:PSS is a water soluble ionic molecule, in which PEDOT acts as the hole carrying semiconductor while PSS serves as a dopant for PEDOT to enhance the dispersion stability. The reason for the choice of PEDOT:PSS to polyaniline is the higher conductivity and higher thermal stability that it possess. HOMO of PEDOT:PSS is aligned around -5.0 eV, and the LUMO is placed around -2.2 eV, provide the polymer both hole transport and electron blocking properties [60,62].

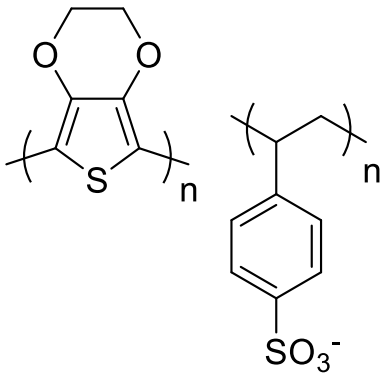

Figure 1.12. Structure of PEDOT:PSS

1.3.1.4. Cathode

For OSCs, cathode serves as the top contact, and the most important aspects of an ideal cathode layer is the high conductivity and relatively lower work function (high electronegativity) to hold the electrons. In this manner, for conventional architecture, metal contacts such as silver (Ag) and aluminum (Al) are used. Ag has a work function around 4.70 eV, which is close to ITO. So that the electron transport through the cathode could be challenging, due to high work function of the metal, without the use of an electron transport layer (ETL). Therefore, before the deposition of Ag layer, there are usually interfacial layers coated onto the active layer. Ag is usually used with calcium (Ca) as the top contact, to reduce the active work function of the Ag layer [63].

Al, is a commonly used metal as the cathode, with a work function of 4.30 eV. Although the work function is quite low, Al is also used via an interfacial layer, which is lithium fluoride. LiF possess a work function around 2.90 eV, which corresponds to an energy level above the LUMO of the acceptor molecule (-3.90 eV for $PC_{71}BM$). As a result, it causes the electron to jump to a higher energy level, which is more excited and less electronegative, during the transportation towards the cathode. Hence, when LiF layer deposition becomes greater than 0.7 nm, LiF begins to bear insulating properties. However, deposition of thin layer LiF before Al deposition is required for reasons other than electron transport. One of the reasons is the high boiling point of Al. At standard conditions, the boiling point of Al is recorded as 2.470 °C, which is much higher than the temperatures that the active layer can tolerate without degrading. Although the Al layer is vacuum deposited and the evaporation temperature is reduced, LiF layer coated onto the active layer prevents hot bombing of the Al metal onto the D-A blend, as a precaution to polymer degradation. In addition, it provides a smooth surface for Al deposition, improving the contact quality between the active layer and the cathode, and reducing the series resistance of the device to improve the overall photovoltaic performance. Lastly, LiF reduces the active work function of Al layer, to decrease the energy barrier between the Al and the LUMO of the acceptor molecule for efficient transport of electrons to the cathode, as an ETL. Lastly, due to very low work function, LiF functions as a hole blocking layer to enhance the shunt resistance [60,64].

1.4. Parameters Affecting the Overall Performance of an OSC

1.4.1. Solar Spectra and Standard Solar Spectrum (AM1.5G)

Solar spectrum changes during day, mainly due to the relative angle of the incoming solar radiation to the Earth surface. There are several solar spectra that are classified due to the angle of incidence and the total intensity of the incoming light. The classification of solar spectra are usually defined in terms of “air mass”, abbreviated as AM, stands for the ratio of the direct optical pathlength that the solar irradiation

follows to the Earth atmosphere, to the vertical path length of solar irradiation to the zenith, where the intensity of the light reaching the atmosphere is the highest. The AM coefficient in the naming of the spectrum, in which AM0 stands for the irradiation following the vertical path from the Sun to the atmosphere. For AM1.5, the angle of the solar irradiance relative to the zenith angle is 48.2°, and as the name recalls, AM coefficient is determined as 1.5. This coefficient can be calculated as the $\cos^{-1}(48.2°)$ for AM1.5 spectrum, and be varied depending on the angle for all other solar spectra. Naming of the spectrum ends with the symbol defining the type of irradiation considered for characterizations. Symbol D stands for direct solar radiation reaching the Earth atmosphere. On the other hand, symbol G stands for the global radiation, which considers the direct solar radiation and the diffuse radiation that includes the reflected and scattered light. For space applications, usually AM0G spectrum, which has the highest intensity of 1366.1 W/m^2 among all solar spectra, is used for standard characterization methods. However, the research on energy production from solar irradiation on Earth by the aid of flat plate modules utilizes the AM1.5G spectrum as the standard conditions, with total intensity of 1000 W/m^2. The absorbable portion of this spectrum mainly covers wavelength region between 300-1000 nm, including the UV-Vis NIR region. As discussed in section 1.3.1.1.1.1., the photocurrent generated is directly related to the portion of the spectrum absorbed, so that for OSCs, narrow band polymers are desired for enhanced absorption of AM1.5G spectrum.

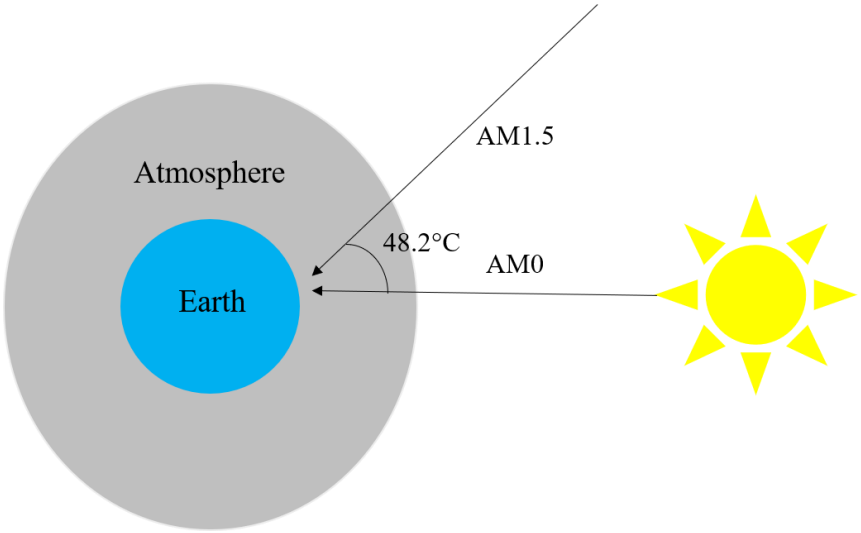

Figure 1.13. AM1.5G standardization

1.4.2. Power Conversion Efficiency (PCE)

Power conversion efficiency, (PCE) is basically the ratio of the maximum power generated by the solar cell to the ratio of the total power applied on the device by the solar spectrum. So that this parameter can be defined as the maximum efficiency of a solar cell. However, in order to fully understand the concept of PCE, some other parameters related to the performance of a solar cell should be defined. The PCE of a solar cell is defined after current-voltage characterization of a solar cell, under AM1.5G illumination. Figure 1.14. illustrates a sample current density-voltage (J-V) curve, including all the parameters that could be defined from it [23].

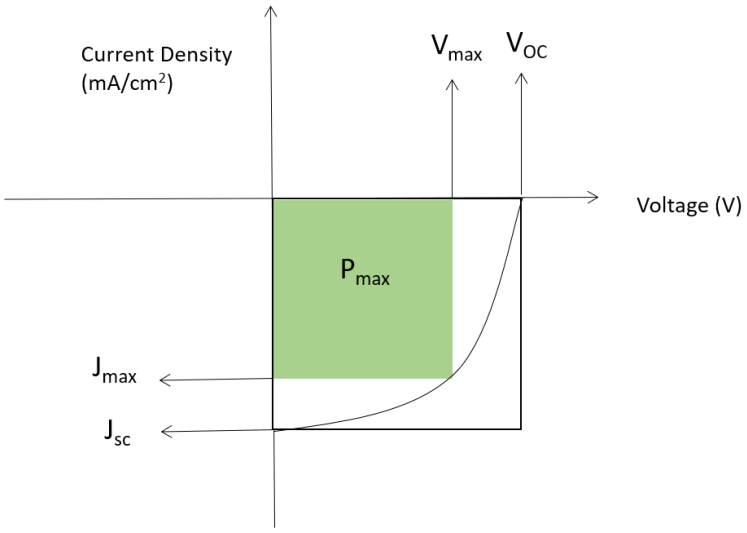

Figure 1.14. Illustration of a sample J-V curve

With all the parameters denoted on Figure 1.14., the PCE can be determined with the use of the following relation:

$$\text{PCE}\% = \frac{P_{OUT}}{P_{IN}} x100 = \frac{FFxJ_{SC}xV_{OC}}{100\ mW/cm^2} x100 = FFxJ_{SC}xV_{OC} \quad (1)$$

These parameters and the factors affecting them should be well understood, in order to determine PCE for a solar cell.

1.4.2.1. Open Circuit Voltage (V_{OC})

As it can be seen in Figure 1.14., open circuit voltage, (V_{OC}) can basically be defined as the voltage recorded when there is no current flow through the system.

$$V_{OC} \approx E_{LUMO,A} - E_{HOMO,D} + k_BT/e\{\ln(n_e n_h/N^2_c)\} \quad (2)$$

Equation 2 is the approximation given for the determination of V_{OC} values [23,65]. $E_{LUMO,A,}$ stands for the LUMO of the acceptor molecule and $E_{HOMO,D}$ stands for the HOMO of the donor molecule. This means that the V_{OC} values for OSCs are mainly determined by the energy difference between the LUMO of the acceptor and HOMO of the donor molecules. Normally, V_{OC} is determined by the difference in the work

functions of the electrodes. However, for the recently developed OSC designs, V_{OC} values are enhanced towards the interfacial layers used in the device architecture, mainly by the active layer. As mentioned previously, in order to prevent losses from $V_{OC,}$ HOMO levels should not be increased excessively to achieve a narrow band gap for conjugated polymers in OSCs. Use of non-fullerene acceptors with alterable LUMO levels is another method to increase V_{OC} for OSCs [44,66].

Other than the HOMO and LUMO levels, V_{OC} values are related to how efficiently charges are collected at the corresponding electrodes. So, the factors that affects the overall photovoltaic performance of an OSC, such as optimum morphology, contact quality between the layers and the charge transport through the device via compatible energy levels is related to high V_{OC} values. Also, high shunt resistance values are required for high V_{OC} values. Shunt resistance basically defines the power loss of a solar cell via leakage of current. This might happen when charges prefer alternative patterns to reach the electrodes. Such situation might result in the collection of the holes at the electrodes, and electrons at the anodes. This would decrease the potential difference created between the electrodes when the light hits the solar cells, leading to lower V_{OC} values. This is why HTL and ETL materials to show electron blocking and hole blocking properties, respectively, is very important. Defect free device processing is also a very important parameter for desirable V_{OC}, as defects directly reduces the work function of the electrodes and materials, and the V_{OC} values negatively [10,67].

1.4.2.2. Short Circuit Current Density (J_{SC})

Short circuit current density (J_{SC}) is defined as the current density measured for a solar cell when there is no external voltage applied. Rather than short circuit current, it is called the current density because it is the current value measured for the area of the solar device. For an OSC, J_{SC} value is mainly related to the absorption of the active layer. So that, as discussed previously, increasing the active layer thickness, D-A blend concentration and enhanced donor molecule loading to the D-A blend

increases the absorption, these applications are expected to enhance the J_{SC} value. However, the parameter is also highly dependent on the effective charge collection on the electrons in addition to the number of excitons formed, so it requires low series and high shunt resistance values. This means, for desirable J_{SC}, all the characteristics defined for an ideal conjugated polymer and ideal, defect free OSC design are required. Note that, high absorption is achieved for low band gap conjugated polymers.

1.4.2.3. Fill Factor (FF)

Fill factor (FF) is a parameter that defines the portion of a solar cell's maximum performance that it can exhibit. The parameter is explained by the following relation:

$$FF = \frac{J_{max} x V_{max}}{J_{SC} x V_{OC}} \quad (3)$$

For an ideal case, the value of FF equals to 1. The ideal condition is pointed by the white region included in the J-V curve given in Figure 1.14. However, the real life case holds as the green box given in the J-V curve illustrated in Figure 1.14., denoted as P_{max}. Maximum power generated by the solar cell is determined by J_{max} and $V_{max,}$ which are lower than the ideal values. All parameters affecting J_{SC} value other than the absorption of the active layer, affects FF values as well. All aspects affect the V_{OC} values other than the difference between $E_{HOMO,A}$ and $E_{LUMO,D}$, and the work functions of the electrodes influence the FF value as well, for OSCs. This is because the high FF values are also related with the collection of the charges at the corresponding electrodes and require low series resistance and high shunt resistance. However, the degree of losses from the already determined J_{SC} and V_{OC} values are determined by the active layer morphology. Thus, FF value is mainly determined by the effective D-A phase separation at the active layer, with an interpenetrated bicontinuous morphology, with optimum domain sizes. As a result, FF is mainly affected by the active layer morphology [10,68].

1.5. Incorporation of π-bridges and Fluorination on Conjugated Polymers

As previously discussed, photovoltaic performance of conjugated polymers can be enhanced by the extension of conjugation length by the incorporation of π-bridges. This enhances the degree of electron delocalization through the polymer backbone, to enhance the electronic properties of the conjugated polymers. In addition, this extension is proved to enhance the intramolecular charge transfer from the electron rich donor unit to electron poor acceptor unit in the polymer backbone [69]. This helps to molecule to perform red-shift in the absorption spectra, to achieve a lower E_g. Thiophene and selenophene units are two types of moieties used commonly for conjugated polymers to serve as π-bridges.

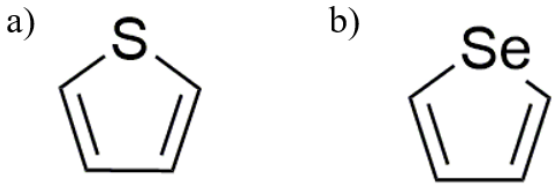

Figure 1.15. Structures of a) thiophene and b) selenophene moieties

Due to more rigid backbone, less aromatic and more quinoid character, recent works have shown that conjugated polymers bearing selenophene units have lower E_g compared to the thiophene comprising ones [70]. Moreover, high polarizable nature of selenophene results in higher charge mobility [71].

In order to tune the energy levels of the frontier orbitals, introduction of the fluorine atom to the polymer backbone is also an emerging method. As the fluorine atom is the most electronegative element and among all the electron withdrawing units it is the smallest one, it does not cause any steric hinderance and yields downshifted HOMO and LUMO levels for the conjugated polymers. This yields higher V_{OC} values for the conjugated polymer based OSCs [72–74].

1.6. Aim of the Study

In this study, photovoltaic characterizations of two fluorine incorporated novel polymers bearing benzothiadiazole and benzotriazole as the acceptor units, and benzodithiophene as the donor unit are aimed to be carried out. Conventional OSC device architecture was used for the characterizations of the polymers. The effect of incorporation of thiophene and selenophene on the band gaps and photovoltaic performance of the polymers were investigated. Electrochemical, optical, spectroelectrochemical, kinetic, thermal and photovoltaic characterizations of the selenophene bearing P1, and thiophene bearing P2 were carried out. Molecular weight values were determined by using the gel permeation chromatography (GPC) technique.

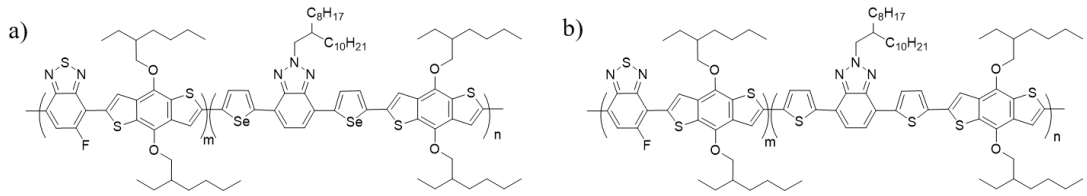

Figure 1.16. Structures of polymers a) P1 and b) P2

CHAPTER 2

EXPERIMENTAL

2.1. Materials and Equipments

Polymers P1 and P2 were synthesized by Duygu Keleş from Çırpan's research group and supplied by the synthesis laboratory. Weight average molecular weight (M_W) values are determined to be 9 kDa and 15 kDa, for P1 and P2, respectively. Polymer films were prepared by coating polymer solutions (2 mg/mL) onto the ITO coated glass substrates. Polymer coated ITO (working electrode), Pt wire (counter electrode), and Ag wire (reference electrode) were placed in a cell containing 0.1 M tetrabutylammonium hexafluorophosphate/acetonitrile ($TBAPF_6$/ACN) mixture. ITO coated glass substrates were supplied from VisionTek Systems. Electrochemical studies were performed with Gamry 600 potentiostat, and an Agilent 8453 spectrometer was used for spectroelectrochemical measurements. PSC device fabrication and characterization were achieved in a glove box system (MBraun). Toluene and 2-propanol used for the ITO cleaning process was supplied from Sigma Aldrich Chemical Co. Ltd. Cleaning detergent was purchased from Hellmanex and PEDOT:PSS 4083 was supplied from Heraeus. Methanol, orthodichlorobenzene, chloronaphthalene and methanol was supplied from Sigma Aldrich Chemical Co. Ltd. LiF and Al were purchased from Kurt J. Lesker. A Perkin Elmer Differential Scanning Calorimetry was used for Differential Scanning Calorimetry (DSC), and a Perkin Elmer Pyris 1 TGA was used for thermogravimetric analyses (TGA) at a heating rate of 10°C/min under nitrogen atmosphere. TEM analysis for morphology imaging was performed by METU Central Laboratory.

2.2. Electrochemical Studies

Polymers P1 and P2 were dissolved in chloroform (2 mg/mL) and spray coated onto the ITO substrate via Omni spray coating gun. In electrochemistry experiments, a three electrode experimental setup was established, in which ITO was used as the working electrode, Ag as the reference electrode and Pt as the counter electrode. Tetrabutylammonium hexafluorophosphate ($TBAPF_6$) was used as the supporting electrolyte, whereas acetonitrile (ACN) was used as the solvent. Cyclic voltammetry (CV) experiment was conducted to carry out the electrochemical studies. Cyclic voltammograms were monitored between suitable potentials for P1 and P2 at a scan rate of 100 mV/s at room temperature. With the CV measurements, HOMO and LUMO levels of the polymers were determined. These values were used to calculate the electronic band gap values for the polymers.

2.3. Optical Studies

Optical properties of polymers were investigated in visible and NIR regions by spectrophotometer. Polymers were dissolved in chloroform ($CHCl_3$) and spin coated on glass substrates to identify the thin film absorption spectra of the polymers. Solution absorption spectra of the polymers were also studied for polymers by spectrophotometer. As a result of optical studies, absorption wavelengths of the polymers were determined to calculate the optical band gap values.

2.4. Spectroelectrochemical Studies

In this experiment, polymer films were exposed to stepwise oxidation potentials. Polymers were dissolved in $CHCl_3$ and spray coated on ITO coated glass substrates. 0.1 M $TBAPF_6$/ACN were used as the supporting electrolyte/solvent system. Three electrode which consists of reference electrode (Ag), counter electrode (Pt), and working electrode (polymer coated ITO) were immersed in supporting electrolyte/solvent.

2.5. Kinetic Studies

In order to investigate optical contrast and switching time of the polymers kinetic studies were carried out. Three electrode system was constructed in a quartz cell as described for the spectroelectrochemistry part.

2.6. Device Fabrication and Characterization

Photovoltaic parameters of P1 and P2 are investigated with the device structure of ITO/PEDOT:PSS (40 nm)/Polymer:$PC_{71}BM$/LiF (0.6 nm)/ Al (10 nm).

2.6.1. ITO Cleaning

ITO glass substrates purchased from Visiontek were etched via zinc powder and hydrochloric acid treatment. This was performed to reduce the active area on the glass substrate, to reduce the possibility of defect formation during device fabrication process. This process was followed by ultrasonication in toluene, detergent, water and isopropyl alcohol respectively. The sonication was carried out for 15 minutes for each solvent indicated. Thereafter, substrates were dried with nitrogen gun and O_2 plasma treatment was performed for 5 minutes. Plasma treatment was performed to enhance the work function of the ITO substrate, to reduce the surface tension of the hydrophobic ITO surface for efficient PEDOT:PSS coating, and mainly, to etch the organic residues remaining on the ITO surface.

2.6.2. PEDOT:PSS Coating

The ITO cleaning process was followed by spin-coating of PEDOT:PSS in an ambient atmosphere G3P Spincoat of Speacilty Coating Systems. The PEDOT:PSS layer was spin coated out of the glove box system, as a precaution to contamination of the system by the water based nature of the PEDOT:PSS solution. The spin coating was carried out at 4000 rpm, for 40 s. Prior to spin coating process, the PEDOT:PSS solution was filtered through the 0.45 μm polyethersulfone (PES) filters. After the layer was coated, baking of the coated substrates at 135°C for 15 minutes was performed, to remove water residue left on the layer.

2.6.3. Active Layer Processing

Polymer:$PC_{71}BM$ blends with different weight ratios, different blend concentrations (w/v) and different solvent additive concentrations (v/v%) were prepared in *o*-dichlorobenzene (o-DCB). Active layers were spin coated in nitrogen filled glove box, with different spin-coating rates to determine the optimum thickness.

2.6.4. Metal Evaporation

0.6 nm LiF and 100 nm Al layers were deposited on the Polymer:$PC_{71}BM$ layer at $2x10^{-6}$ mbar, inside the glove box. The metal deposition was performed in a vacuum evaporation chamber to reduce the processing temperatures, as metal evaporation takes place at excessive temperatures that can degenerate the active layer. Deposition rates were monitored by Inficon SQC-310 Thin Film Deposition Controller.

2.6.5. Photovoltaic Characterization of OSCs

Photovoltaic measurements of the devices were performed inside the glove box under the illumination of AM 1.5G. The measurements were done by Keithley 2400.

CHAPTER 3

RESULTS AND DISCUSSION

3.1. Electrochemical Studies

Electrochemical properties of the polymers were investigated via cyclic voltammetry (CV) experiments. The polymers were dissolved in chloroform and spray coated onto ITO electrodes, and the experiments were conducted by a three electrode system as explained in section 2.1. As depicted in Figure 3.1. both P1 and P2 showed ambipolar character, which means they are both n- and p-dopable.

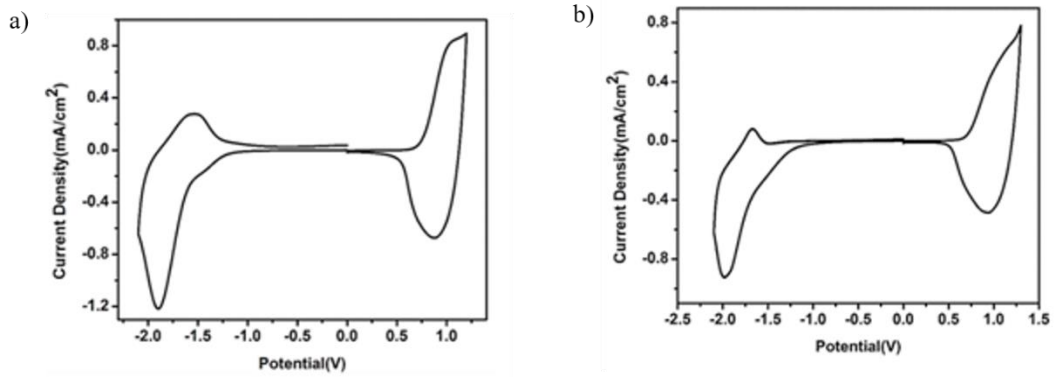

Figure 3.1. Cyclic voltammograms of a) P1 and b) P2, in 0.1 M $TBAPF_6$/ACN at 100 mV/s scan rate

The ambipolar character that these polymers showed can be correlated to the incorporation of the thiophene and selenophene π bridge to the polymer backbone. Polymers with the same backbone without π bridge incorporation have been previously studied by Keleş et al. [75], with and without fluorine introduction, and the polymers were proven to be only p-dopable . The contribution of π bridge introduction to the n-doping process is that the improvement of the ion diffusion. π

bridge incorporation ease the dopant ion insertion and may render n doping process possible.

P doping redox couples were recorded as 1.05 V/ 0.87 V and 1.18 V/ 0.93 V for P1 and P2, respectively. On the other hand, redox couples are at -1.90/ -1.55 V and -1.98/ -1.68 V during n-type doping, respectively. Stronger electron donating ability of selenophene increases the electron density on the main chain resulting in lower oxidation potential.

HOMO and LUMO energy levels were calculated from oxidation and reduction the onset potentials according to following equations;

$$HOMO = -(4.75 + E_{ox}^{onset}) \text{ eV} \quad (4)$$

$$LUMO = -(4.75 + E_{red}^{onset}) \text{ eV} \quad (5)$$

The value 4.75 corresponds to the HOMO level of ferrocene, which is recorded as -4.80 eV below the vacuum level. The value is reduced to 4.75, as the half wave potential for the ferrocene/ferrocenium (Fc/Fc^+) redox couple was estimated as 0.05 eV. Such modification is required for the HOMO and LUMO measurements of the polymers, as the silver (Ag) wire used reference electrode was calibrated against the Fc/Fc^+ electrolyte [76,77].

Owing to ambipolar features of P1 and P2, both HOMO and LUMO energy levels were determined using cyclic voltammetry studies. While HOMO and LUMO energy levels were calculated for P1 as -5.45/ -3.25 eV, they were -5.46/ -3.19 eV for P2. Onset potentials for both oxidation and reduction processes are used for the calculation of HOMO and LUMO levels. Onset potential is the potential measured where the oxidation or reduction process is initiated and measured at the point where the tangent to the oxidation or reduction peak intersects the current density value of zero. The oxidation onset potential (E_{ox}^{onset}) for P1 was measured as 0.70 V, while reduction onset potential was measured as (E_{red}^{onset}) as -1.50 V. The values were recorded as 0.71 and -1.56 for E_{ox}^{onset} and E_{red}^{onset} of P2, respectively. The electronic

band gap (E_g^{el}) values were also calculated by measuring the difference between the HOMO and LUMO levels both for P1 and P2, as 2.20 eV and 2.27 eV, respectively. According to these results, selenophene-based polymer P1 has lower band gap than thiophene-based polymer P2. Similar to previous studies, with the insertion of selenophene instead of thiophene resulting in decrease in LUMO level without changing the HOMO level [78–80]. The results of CV analyses were summarized in Table 3.1.

Table 3.1. Summary of electrochemical and optical properties of P1 and P2

Polymer	$E_{p\text{-doping}}$ (V)	$E_{n\text{-doping}}$ (V)	E_{ox}^{onset} (V)	E_{red}^{onset} (V)	HOMO (eV)	LUMO (eV)	E_g^{el} (eV)
P1	1.05	-1.90	0.70	-1.50	-5.45	-3.25	2.20
P2	1.18	-1.98	0.71	-1.56	-5.46	-3.19	2.27

3.2. Optical Studies

Both thin film and solution absorption spectra of polymers P1 and P2 were investigated in the visible and NIR regions with spectrophotometer, as described in section 2.2. When the absorption spectra of the polymers observed, there is a significant difference observed between P1 and P2. While P1 showed a peak at 605 nm with a shoulder at 560 nm, P2 showed a peak at 565 nm with a shoulder at 535 nm. P3 has red shifted absorption spectrum compared to P2. Shorter wavelength absorption can be assigned to π-π* transition, absorption at longer wavelengths can be assigned to intramolecular charge transfer (ICT) between the electron-rich and electron-deficient units [81]. In Figure 3.2., it can be inferred that the absorption spectrum was red shifted for P1 compared to P2. The main reason for this red-shift performed by P1 is the incorporation of electron rich selenophene moiety to the polymer backbone, instead of relatively electron poor thiophene unit.

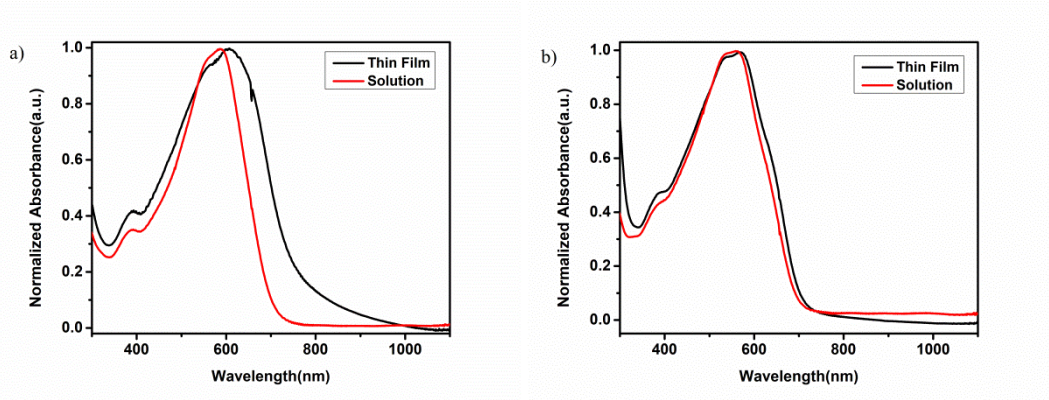

Figure 3.2. UV-Vis normalized absorption spectra of in $CHCl_3$ solution and film for a) P1 and b) P2

As depicted in Figure 3.2., all polymers showed broad absorption in visible region. There is no significant red-shift in thin film absorption compared to that of solution absorption for P2, which proves the minority of the aggregation in thin film [82,83]. The red-shift observed for the thin film for the selenophene bearing P1 signals the formation of aggregation. This aggregation is mainly formed due to the quinoidal character of the selenophene moieties, as the larger size of selenium compared to sulfur results in lower aromaticity of the unit. Lower aromaticity is a result of poor overlapping of the selenium orbitals with the carbon framework forming the π-system. As a result, the dominating intermolecular interactions between the polymer chains are most probably the π-π stacking, resulting in film aggregation. Hence, a red-shift is absorbed for thin film absorption spectrum of P1, compared to the spectrum of the solution [38,84].

Optical band gaps were determined from the λ_{max}^{onset} values, which is the onset absorption wavelength, and defined as the wavelength value where the absorption process is initiated for a given polymer. The values were recorded as 760 nm for P1 and 715 nm for P2. Optical band gaps for P1 and P2 are calculated as 1.63 eV and 1.73 eV, respectively. Results of optical studies were given in Table 3.2, electronic band gap (E_g^{el}) values are higher than E_g^{op} for both polymers due to the free electrons in the electrochemistry experiment [85].

Calculation of the E_g^{op} by using λ_{max}^{onset} values was performed by using the following equation;

$$E_g^{op} = \frac{1241}{\lambda_{onset}} \quad (6)$$

This formula basically arises from Planck's law, that is used to calculate the total energy of a photon related to its wavelength. Band gap values are calculated in terms of eV, so that the constant 1241 is basically the conversion of the multiplication of Planck's constant and speed of light (h x c), in terms of eV. As the absorption spectrum of the polymer corresponds to the excitation of the electron from HOMO to LUMO, the energy corresponds to the absorbed wavelength directly labeled as the optical band gap of the polymer.

When the E_g^{op} values of both polymers are compared, selenophene bearing P1 possessed a reduced band gap compared to the thiophene bearing P2, as the values were recorded as 1.63 eV and 1.73 eV, respectively. This phenomenon can be explained by the π-π stacking performed by selenophene moiety, due to previously clarified reasons, causing a redshift in the overall absorption spectrum of the polymer. Electronic band gap (E_g^{el}) value given in Section 3.1 was also recorded lower for P1 compared to that of P2, due to lowered LUMO levels, in the presence of selenophene moiety. Thus, the electrochemical and optical studies verified each other on this manner. The parameters measured by optical studies are summarized in Table 3.2.

Table 3.2. Summary of electrochemical and optical properties of P1 and P2

Polymer	λ_{max} (nm)	λ_{max}^{onset} (nm)	E_g^{op} (eV)
P1	605	760	1.63
P2	565	715	1.73

3.3 Spectroelectrochemical Studies

Experimental setup consisting three electrode system, ITO as the working electrode, Pt wire as the counter electrode and Ag wire as the reference electrode was explained in Section 2.4. The spectroelectrochemical studies were carried out to investigate the changing absorption spectra of the polymers upon applied potential. When the potential was applied, intensity of absorption of neutral state was depleting while formation of polaron bands around 800 nm were observed. Polymers have isosbestic points where interconversion of the polymer from their neutral states to the oxidized states [86] at 710 nm for P1 and 655 nm for P2**,** respectively.

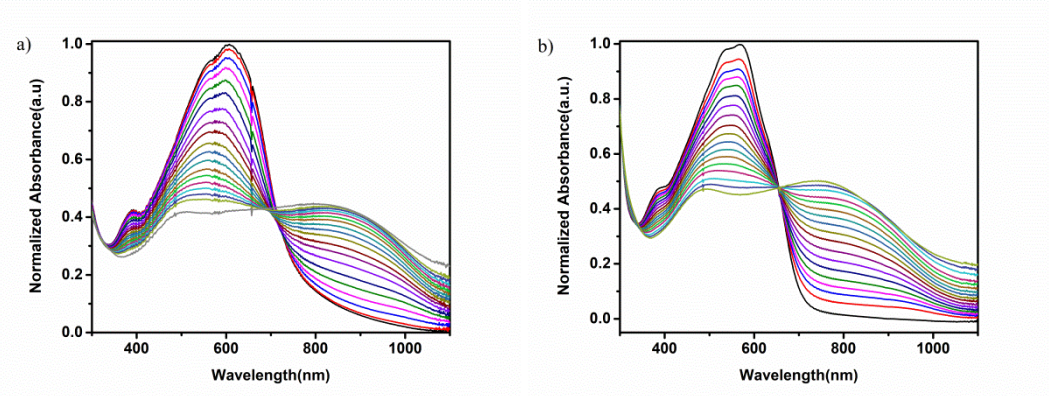

Figure 3.3. Electronic normalized absorption spectra of polymer films recorded at various potentials for a) P1 and b) P2 in 0.1 M $TBAPF_6$/ACN solution

As is depicted in Figure 3.3., the red shift for the absorption spectrum of the selenophene bearing P1 compared to thiophene bearing P2 can be observed. Hence, the results are compatible with the results of the optical studies discussed in Section 3.2. The depletion of the neutral state absorption intensity and formation of the polaron bands around 800 nm upon continuously applied potential can be correlated to the decrease in the concentration of the neutral polymers, and enhancement in the polaron concentration. This is due to continuous oxidation of the polymers via applied potential difference.

3.4. Kinetic Studies

In order to investigate optical contrast and switching time of the polymers kinetic studies were carried out. Optical contrast is the percent transmittance change between the neutral and fully oxidized states of a material at a given wavelength. The time required for switching between these states is defined as the switching time. In the literature, switching time is calculated from 95% of the full contrast since human eye is insensitive to 5% of color change [87]. Three electrode system was constructed in a quartz cell as described for the spectroelectrochemistry part. Then, absorption spectrum was recorded by applying square-wave potential between neutral and fully oxidized states with 5 s time internals (Figure 3.4.). This measurement was repeated for the wavelengths where polymers showed maximum absorption.

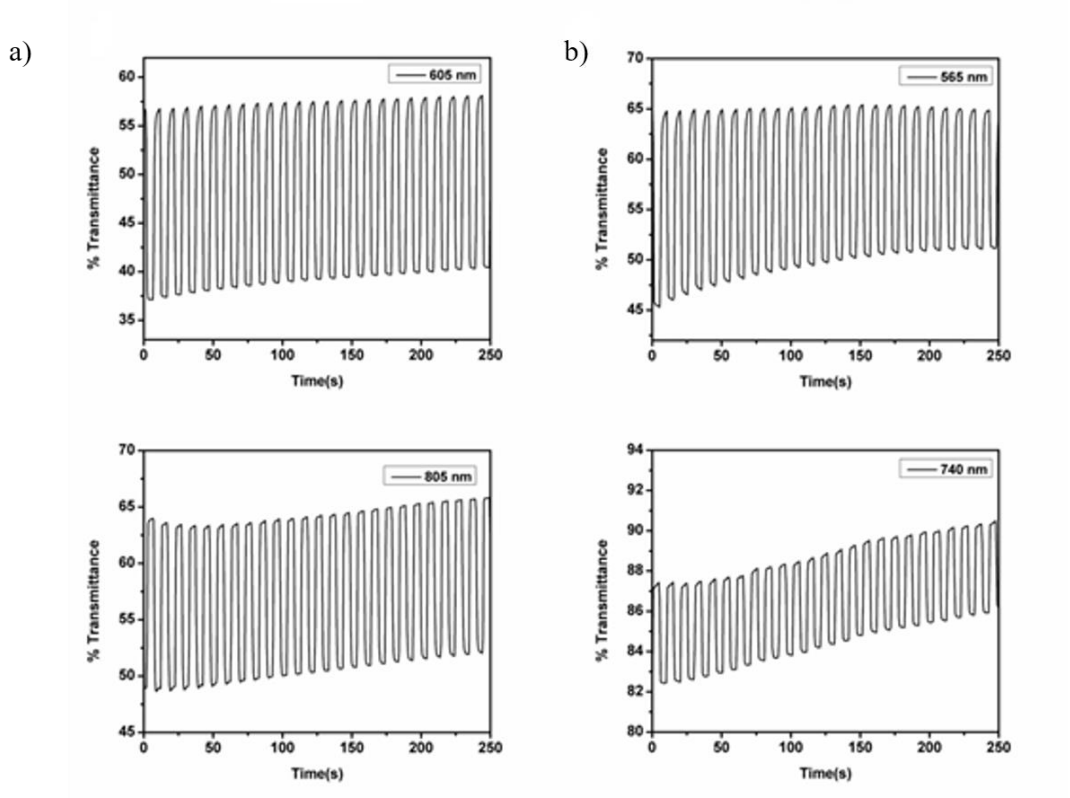

Figure 3.4. Percent transmittance changes of a) P1 and b) P2 in 0.1 M $TBAPF_6$/ACN solution

Table 3.3. summarizes the kinetic parameters of the polymers. Optical contrast of the polymers in the visible region are close to each other. In the NIR region, the highest optical contrast was observed for P1 with 19%.

Table 3.3. Summary of the kinetic studies of the polymers

Polymer	Wavelength (nm)	Optical Contrast (ΔT%)	Switching Time (s)
P1	605	21	1.7
	805	19	1.1
P2	565	23	2.2
	740	7	0.8

3.5. Thermal Studies

Differential scanning calorimetry (DSC) was used to determine thermal transitions. Polymers did not show any phase transition and significant degradation up to 300°C. Thermal stability of the polymers was investigated with thermogravimetry analyses (TGA). These analyses showed that decomposition temperatures of P1 and P2 were at 331°C and 326°C, respectively.

3.6. Photovoltaic Studies

Organic solar cells were constructed using P1 and P2 as the electron donors with the conventional device architecture; ITO/PEDOT:PSS/Polymer:$PC_{71}BM$/LiF/Al. Several optimizations were performed, including the Polymer:$PC_{71}BM$ blend ratio (w/w), blend concentration, spincoating rate (thickness optimization) and addition of DIO (1,8-diiodooctane). In addition to DIO addition, effect of chloronaphthalene (CN) as an additive, thermal annealing and methanol treatment were also examined, however there have been no enhancement for the photovoltaic performance of the polymers. In figure 3.5., the energy level diagram for the P1 and P2 based organic solar cells with the conventional device architecture is illustrated. The energy levels were determined via HOMO, LUMO and electronic band gap measurements conducted in electrochemical studies, given in Section 3.1.

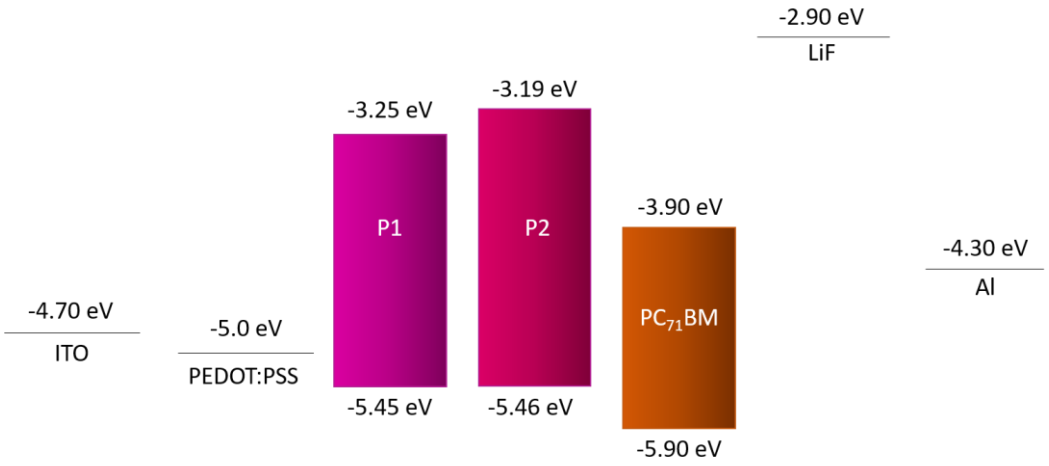

Figure 3.5. Energy level diagram for P1 and P2 based OSCs with conventional device architecture

For the work function values of ITO, PEDOT:PSS, LiF and Al, and the HOMO-LUMO levels of $PC_{71}BM$, the values previously determined for the works performed by Toppare and Çırpan Research group [60].

Table 3.4. and 3.5. summarizes the photovoltaic properties for P1 and P2 respectively, including the previously mentioned optimizations performed.

Table 3.4. Summary of the photovoltaic properties of polymer P1

Polymer(P1):$PC_{71}BM$ (w:w)	J_{sc} (mA/cm^2)	V_{oc} (V)	J_{max} (mA/cm^2)	V_{max} (V)	FF%	η%	RPM	Treatment
1:2 (2%)	4.24	0.66	3.01	0.48	51.63	1.44	750	-
1:3 (2%)	**3.80**	**0.65**	**3.02**	**0.51**	**62.36**	**1.60**	**750**	**-**
1:4 (2%)	3.84	0.64	3.06	0.50	62.26	1.56	750	-
1:3 (3%)	3.55	0.63	2.93	0.46	61.86	1.35	750	-
1:3 (3%)	3.64	0.66	2.78	0.52	60.17	1.43	1000	-
1:3 (2%)	2.99	0.60	2.41	0.46	61.79	1.11	1000	-
1:3 (2%)	4.14	0.57	3.12	0.45	59.50	1.40	750	2% DIO
1:3 (2%)	3.47	0.55	2.70	0.43	60.83	1.15	750	3% DIO
1:3 (2%)	3.92	0.59	3.12	0.44	59.36	1.37	750	3% CN

Table 3.5. Summary of the photovoltaic properties of polymer P2

Polymer(P2):$PC_{71}BM$ (w:w)	J_{sc} (mA/cm^2)	V_{oc} (V)	J_{max} (mA/cm^2)	V_{max} (V)	FF%	η%	RPM	Treatment
1:2 (2%)	3.44	0.75	2.05	0.48	38.14	1.04	750	-
1:3 (2%)	4.38	0.71	3.57	0.55	63.14	1.75	750	-
1:4 (2%)	4.22	0.70	3.02	0.54	55.21	1.64	750	-
1:3 (3%)	5.52	0.77	4.31	0.61	61.86	2.65	750	-
1:3 (3%)	6.14	0.76	4.87	0.60	62.62	2.91	500	-
1:3 (3%)	5.99	0.76	4.71	0.62	64.15	2.93	1000	-
1:3 (3%)	8.30	0.65	6.38	0.44	52.03	2.79	500	3% DIO
1:3 (3%)	9.23	0.65	7.19	0.47	56.33	3.38	500	4% DIO
1:3 (3%)	**8.83**	**0.66**	**7.28**	**0.53**	**66.21**	**3.83**	**1000**	**4% DIO**

In both tables, Table 3.4. and Table 3.5., the symbol η stands for the power conversion efficiency (PCE) of the OSCs. As it can be seen in Table 3.4., for P1 based OSCs, when the polymer:$PC_{71}BM$ ratio was altered from was changed from 1:2 to 1:3, there was a decrease in the short circuit current (J_{SC}) value, 4.24 mA/cm^2 to 3.80 mA/cm^2. This could be explained by the enhanced $PC_{71}BM$ loading. In other words, as the polymer concentration inside the blend was decreased, reduced ability of the active layer to harvest the irradiated light might have caused a reduction in the current values. As mentioned previously, J_{SC} values are mainly determined by the absorption intensity of the active layer, which is mostly performed by the polymers as $PC_{71}BM$ have low absorptivity coefficients towards AM1.5G. Although the J_{SC} values are decreased, the PCE values were enhanced from 1.44% to 1.60% when the blend ratio was changed from 1:2 to 1:3. As it can be inferred from Table 3.4., this was mainly provided through a rise in fill factor (FF) values, from 51.63 to 62.36%. As FF values are primarily affected by the active layer morphology, the increase in

PCE and FF as the blend ratio is manipulated can be correlated to the improved morphology of the active layer. The polymer:$PC_{71}BM$ ratio optimization was continued with the characterization of the OSC bearing active layer with a blend ratio of 1:4. J_{SC}, V_{OC} , FF and PCE values were found to be very close to each other, however, through a slight difference in FF values, which has the values 62.36% for 1:3 and 62.26% for 1:4 blend ratio, ratio of 1:3 possessed higher PCE with 1.60%. As a result of polymer:$PC_{71}BM$ ratio optimizations, ratio of 1:3 was found to be optimum blend ratio for the active layer with an active layer thickness of 72 nm, J_{SC} of 3.80 mA/cm^2, V_{OC} of 0.65 V, FF% of 63.14% and PCE% of 1.60%.

The polymer:$PC_{71}BM$ ratio optimization was followed by the optimization of blend concentration. Ratio optimizations were carried out at 2% blend concentration, which is expressed in terms of weight/volume (w/v) concentration of the blend solution. 2% means that the quantity of polymer:$PC_{71}BM$ blend dissolved in 1 mL orthodichlorobenzene (o-DCB) is 20 mg. Hence, 2% corresponds to a concentration of 20 mg/mL, while 3% blend concentration stands for 30 mg/mL polymer:$PC_{71}BM$ blend dissolved in o-DCB. When the photovoltaic characterization of the active layer processed from a solution with blend concentration of 3%, the aim is mainly to achieve an increase in current density values due to enhanced absorption of the incoming radiation. However, both J_{SC} and FF values were decreased compared to the device processed from 2% blend concentration. Reduction of J_{SC} from 3.80 mA/cm^2 to 3.55 mA/cm^2 which causes the reduction of PCE% from 1.60% to 1.35% might have caused due to excessive thickness of the active layer. As both solutions were spin coated at 750 rpm, the layer processed from higher concentration blend is expected to have a higher thickness. Thicker layer obtained for the blend concentration of 3% might have caused non-geminate recombination processes, as the charges fail to reach the corresponding electrodes as the pathway is enhanced. To achieve thinner layer with this estimation, polymer:$PC_{71}BM$ blend solution with the same concentration was processed with higher spincoating rate, as the rate was increased from 750 rpm to 1000 rpm. As it is stated in Table 3.4., the PCE% value

was enhanced to 1.43% from 1.35%. As thinner layers yielded higher photovoltaic performance, blend solution with optimum concentration, 2% was processed at 1000 rpm as well. However, J_{SC} value decreased from 3.80 mA/cm^2 to 2.99 mA/cm^2 for 2% blend concentration, from the spin coating rate of 750 rpm to 1000 rpm. This caused a decrease in PCE% from 1.60% to 1.11%. Hence, the optimum conditions for the P1 based OSCs were determined to be the device constructed with a solution with a polymer:$PC_{71}BM$ ratio of 1:3 and blend concentration of 2% processed at a spin coating rate of 750 rpm. The effects of the introduction of the DIO and CN additives to the active layer to the photovoltaic performance of the P1 based OSCs were also investigated. Both additives improved the J_{SC} values however, resulted in a decrease in overall efficiency of the devices, through a drop in V_{OC} and FF values. This signals the deformation of the active morphology upon additive treatment, which will be further discussed for the TEM image analysis of the active layers processed.

Table 3.5. summarizes the photovoltaic optimizations of P2. Upon polymer:$PC_{71}BM$ ratio optimization of the polymer, blend ratio of 1:3 was found to be the optimum ratio. As the highest J_{SC} value was obtained for 1:3 ratio, as 4.38 mA/cm^2, the main difference between different ratios was recorded as the FF values obtained. As the ratio was altered from 1:2 to 1:4, the FF values were calculated as 38.14%, 63.14% and 55.21%, respectively. This signals that the optimum morphology was achieved for the active layer bearing polymer:$PC_{71}BM$ ratio of 1:3, with a J_{SC} of 4.38 mA/cm^2, V_{OC} of 0.75 V, FF of 63.14% and a PCE of 1.75%. Increase in blend concentration from 2% to 3% yields to a thicker active layer and a rise in PCE significantly to 2.91%. Similar to previous publications, increasing active layer thickness results in J_{SC} raise. This is mainly due to the active layer's enhanced capacity of harvesting sun light [88,89]. After blend concentration was optimized, thickness optimization was performed by processing of the solutions at different spin coating rates. OSCs processed at both 1000 rpm and 500 rpm possessed higher PCE values compared to the device processed at 750 rpm, recorded as 2.91% and 2.93%,

respectively. Reducing the coating rate to 500 rpm, yields a thicker compared to device processed at 750 rpm, increasing the J_{SC} value from 5.52 mA/cm^2 to 6.14 mA/cm^2, due to increased ability to harvest the irradiated light. For the device processed at 1000 rpm, current density reduced to 5.99 mA/cm^2 due to formation of a thinner film, however, the FF value was achieved to be highest among the all the devices processed at different spin coating rates, with the value of 64.15%. This rise could be correlated to the improved morphology with effective phase separation, in other words, formation of bicontinuous interpenetrating network between the donor and acceptor molecules. However, as the effective parameter being studied was thickness, formation of thinner films probably reduced the distance for the separated charges to reach the interfacial layers and eased the effective collection of charges at the corresponding electrodes. As a result, without any additive treatment, the active layer for the P2 based OSCs was determined to be the layer processed from a solution bearing a donor acceptor ratio of 1:3, blend concentration of 3%, at a spin coating rate of 1000 rpm. The mentioned conditions yielded a active layer thickness of 112 nm, and a PCE of 2.93% with a V_{OC} value of 0.76 V.

With 4% DIO addition, performance of P2 based OSC was enhanced and yielded a PCE of 3.83 % through a rise in J_{SC} and FF values. The enhancement of the J_{SC} value to 8.83 mA/cm^2, and of the FF value to 66.21% proves the formation of improved morphology upon additive treatment. The photovoltaic characterization of the best performing OSC constructed via 4% DIO additive treatment of the active layer yielded a V_{OC} of 0.66 V. The morphology improvement will be further discussed in terms of TEM images of the corresponding active layer compositions.

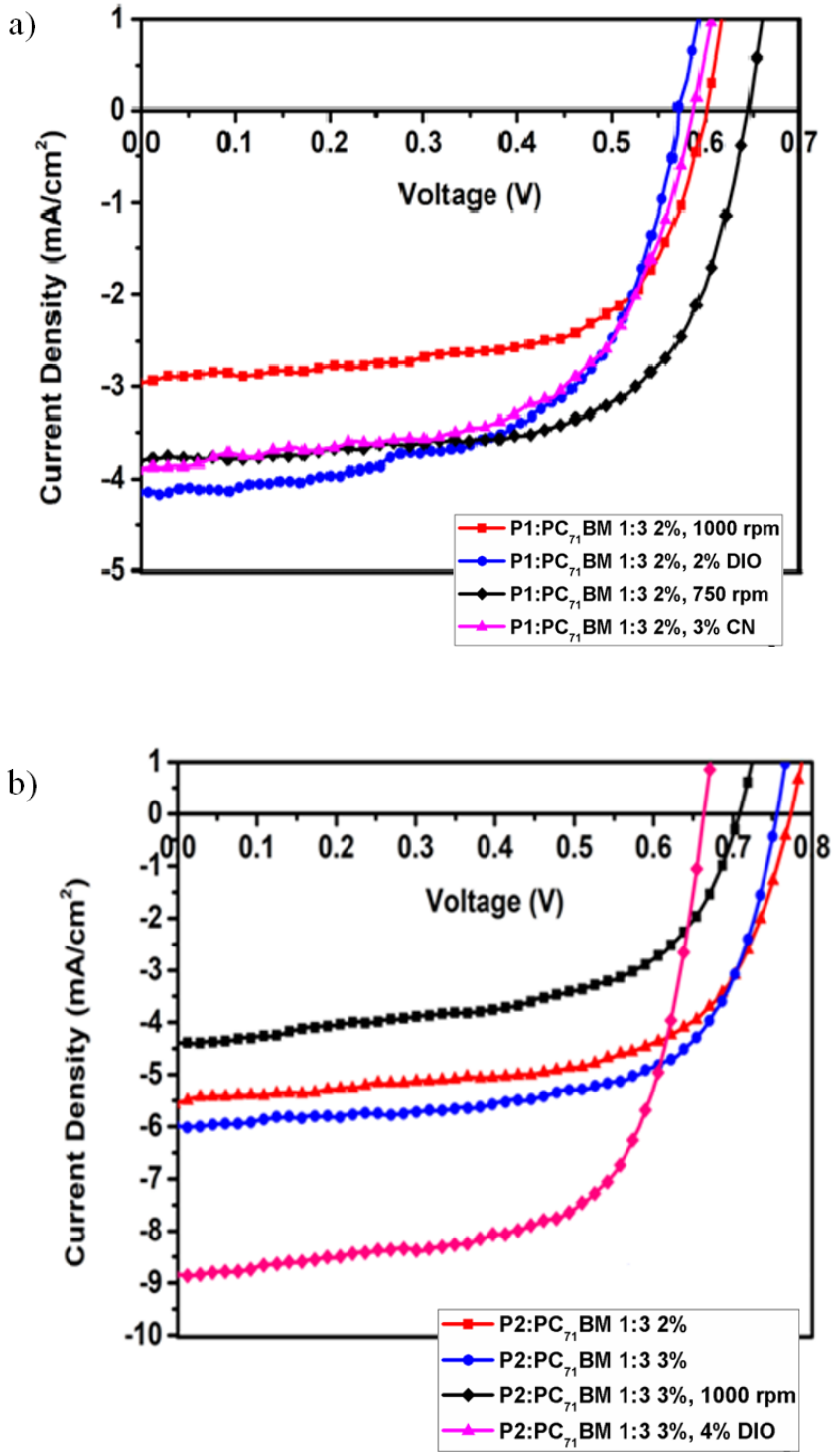

Figure 3.6. J-V curves that summarize photovoltaic performance of (a) P1 and (b)

Figure 3.6. illustrates the J-V curves summarizing the photovoltaic performance of polymers P1 and P2. When the photovoltaic characterizations of both polymers are analyzed, the common parameter that reduces upon additive treatment glitters as $V_{OC.}$ For P1, the value was reduced from 0.65 V to 0.55 V, while the same parameter was reduced from 0.76 V to 0.66 V. This might have caused by the additive residues left in the active layer morphology, creating charge traps, by saturating the conjugated polymers or being trapped in $PC_{71}BM$ [90]. This problem could be handled via methanol treatment to remove the additive residue [91], however methanol treatment resulted in removal of polymer film.

When the V_{OC} values are compared for P1 and P2 based OSCs, processed from o-DCB without any additive treatment, the value was measured as 0.76 V for P2, while it was recorded as 0.66 V for P1. The results given in Section 3.1. for the electrochemical studies shown that the polymers possess similar HOMO levels, so the V_{OC} values should remain similar. Lower value achieved for P1 implies that the charge collection process is less efficient for the polymer, compared to polymer P2. Overall photovoltaic performance of P2 was found to be better compared to selenophene bearing P1, in which the PCE was calculated as 3.83% for P2, while the same parameter was found to be 1.60%. These results are not compatible with the superiorities that selenophene moieties possess, in terms of band gap properties due to the characteristics mentioned previously, and enhanced charge mobilities due to more rigid backbone it contains. Hence, morphological properties of the polymers should be investigated in detail.

To gain more insight into the active layer morphologies, TEM analyses were carried out. TEM images of active layers are shown in Figure 3.7. Both P1 and P2, are low molecular weight polymers with weight average molecular weight values of 9 kDa and 15 kDa, respectively. In consequence, both polymers have excessive solubility which leads to the formation of wider fibrils [40], as seen in Figures 3.7.a and c. Morphology of the P2:$PC_{71}BM$ layer (Figure 3.7.c) was improved with the addition of DIO (Figure 3.7.d). As depicted in Figure 3.7.d, with the addition of DIO to the

P2:$PC_{71}BM$ (Figure 3.7.c) blend, narrower fibrillary structures, where excitons are more likely to reach donor acceptor interface, were formed [40]. Lower photovoltaic performance of P1 based OSCs may be due to the wide fibrils observed in Figure 3.7.a.

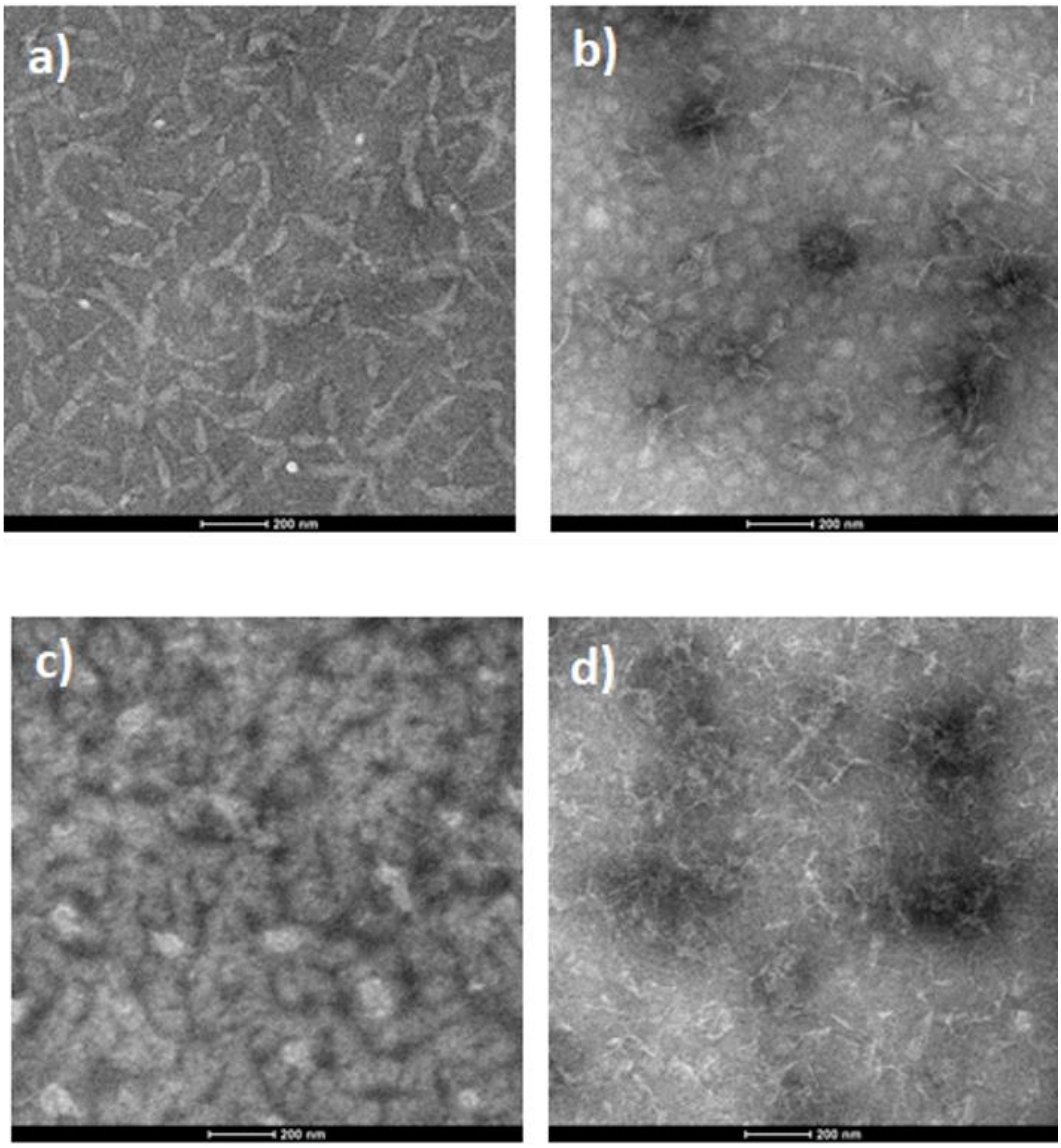

Figure 3.7. TEM images of a) P1:$PC_{71}BM$ processed from o-dcb b) P1:$PC_{71}BM$ processed from o-dcb with 2% DIO, c) P2:$PC_{71}BM$ processed from o-dcb d) P2:$PC_{71}BM$ processed from o-dcb with 4% DIO

In addition to the wider fibrillary structures formed for the morphology of P1 based active layer that interferes the exciton diffusion to the donor acceptor interphase, lower photovoltaic performance of the polymer compared to P2 can also be correlated to the formation of less interpenetrated donor acceptor network (Figure 3.7.a). The bicontinuous interpenetrated donor acceptor phase separation is more obvious for the blend morphology of P2 (Figure 3.7.3), which might have enhanced the efficiency of exciton dissociation and charge transportation of the electrons. This also explains the lower V_{OC} values that P1 based OSCs attains, as charge recombination and trapped charges are more likely for the morphology that the polymer possess. Moreover, reduced efficiency of photovoltaic performance of P1 based OSCs upon additive addition can be correlated to the loss of percolations depicted in Figure 3.7.b, that obstructs the charge transport towards the electrodes. As a result, thiophene bearing polymer P2 achieved better blend morphology upon additive treatment, selenophene bearing P1 additives achieved deformed blend morphology with additive treatment.

In the work of Duygu Keleş et al, photovoltaic performance of the polymers with the same backbone that P1 and P2 possess, without π-bridge incorporation, were investigated [75]. Although the polymers did not bear any π-bridge in their backbone, they possessed higher photovoltaic performance compared to P1 and P2, due to their higher weight average molecular weight values which lead the formation of narrower fibrils in the active layer morphology. The PCE values reaching 4.10% were achieved for those polymers. Structure of the polymers, weight average molecular weight values, TEM images and the best results obtained from their photovoltaic characterizations are included in Appendix A.

CHAPTER 4

CONCLUSIONS

Electrochemical, optical, spectroelectrochemical, kinetic, thermal and photovoltaic studies were carried out for two novel benzotriazole and benzothiadiazole bearing conjugated polymers. Selenophene and thiophene π-bridge incorporated polymers were denoted as P1 and P2, respectively. Thermal studies approved that the polymers are thermally stable up to 300°C. Electrochemical studies showed that both polymers possess ambipolar character. For P1 and P2, the frontier orbital energy levels were calculated as -5.45/-3.25 eV, and -5.46/-3.19 eV respectively. E_g^{op} values were calculated as 1.63 eV for P1 and 1.73 eV for P2. Lower E_g^{op} value achieved for P1 was due to the presence of selenophene moiety in the polymer backbone. Highest PCE values were recorded as 1.60% and 3.83% for P1 and P2 based OSCs, respectively. Formation of wider fibrils lead to a decrease in PCE of the P1 and P2 based OSCs. Improved morphology of thiophene bearing P2 as a result of additive treatment lead to a superior PCE% value compared to selenophene bearing P1. Loss of percolations as a results of additive treatment lead to a decrease in PCE through a decrease in FF, which prevents the improvement of photovoltaic performance, for P1 based OSCs. Complete work based on this thesis was published in the journal Renewable Energy on 18.03.2019.

REFERENCES

[1] D. K. Gupta, M. Langelaar, M. Barink, and F. Van Keulen, “Optimizing front metallization patterns : Ef fi ciency with aesthetics in free-form solar cells,” *Renew. Energy*, vol. 86, pp. 1332–1339, 2016.

[2] M. Höök and X. Tang, “Depletion of fossil fuels and anthropogenic climate change-A review,” *Energy Policy*, vol. 52, pp. 797–809, 2013.

[3] K. E. Trenberth and J. T. Fasullo, “Global warming due to increasing absorbed solar radiation,” *Geophys. Res. Lett.*, vol. 36, no. 7, pp. 1–5, 2009.

[4] P. V. Kamat, “Meeting the clean energy demand: Nanostructure architectures for solar energy conversion,” *J. Phys. Chem. C*, vol. 111, no. 7, pp. 2834–2860, 2007.

[5] K. B. Wolfstirn, “Hole and electron mobilities in doped silicon from radiochemical and conductivity measurements,” *J. Phys. Chem. Solids*, vol. 16, no. 3–4, pp. 279–284, 1960.

[6] V. Alex, S. Finkbeiner, and J. Weber, “Temperature dependence of the indirect energy gap in crystalline silicon,” *J. Appl. Phys.*, vol. 79, no. 9, pp. 6943–6946, 1996.

[7] M. Taguchi, A. Yano, S. Tohoda, K. Matsuyama, Y. Nakamura, T. Nishiwaki, K. Fujita, and E. Maruyama, “24.7% Record efficiency HIT solar cell on thin silicon wafer,” *IEEE J. Photovoltaics*, vol. 4, no. 1, pp. 96–99, 2014.

[8] F. Alharbi, J. D. Bass, A. Salhi, A. Alyamani, H. C. Kim, and R. D. Miller, “Abundant non-toxic materials for thin film solar cells: Alternative to conventional materials,” *Renew. Energy*, vol. 36, no. 10, pp. 2753–2758, 2011.

[9] K. R. Catchpole and A. Polman, “Plasmonic solar cells,” *Opt. Express*, vol. 16, no. 26, p. 21793, 2008.

[10] H. Hoppe and N. S. Sariciftci, “Organic solar cells: An overview,” *J. Mater. Res.*, vol. 19, no. 7, pp. 1924–1945, 2004.

[11] H. Shirakawa, E. J. Louis, A. G. MacDiarmid, C. K. Chiang, and A. J. Heeger, “Synthesis of electrically conducting organic polymers: Halogen derivatives of polyacetylene, (CH)x,” *J. Chem. Soc. Chem. Commun.*, no. 16, pp. 578–580, 1977.

[12] W. Li, B. Guo, C. Chang, X. Guo, M. Zhang, and Y. Li, “Efficient polymer solar cells based on a copolymer of: Meta -alkoxy-phenyl-substituted benzodithiophene and thieno[3,4- b] thiophene,” *J. Mater. Chem. A*, vol. 4,

no. 26, pp. 10135–10141, 2016.

[13] T. K. Das and S. Prusty, “Review on Conducting Polymers and Their Applications,” *Polym. - Plast. Technol. Eng.*, vol. 51, no. 14, pp. 1487–1500, 2012.

[14] R. J. Mortimer, D. R. Rosseinsky, and P. M. S. Monk, *Electrochromic Materials and Devices*. Electrochromic Mater. Devices, 2015.

[15] T. H. Le, Y. Kim, and H. Yoon, “Electrical and electrochemical properties of conducting polymers,” *Polymers (Basel).*, vol. 9, no. 4, 2017.

[16] J. L. Bredas and G. B. Street, “Polarons, Bipolarons, and Solitons in Conducting Polymers,” *Acc. Chem. Res.*, vol. 18, no. 10, pp. 309–315, 1985.

[17] J. Jensen, M. Hösel, A. L. Dyer, and F. C. Krebs, “Development and manufacture of polymer-based electrochromic devices,” *Adv. Funct. Mater.*, vol. 25, no. 14, pp. 2073–2090, 2015.

[18] M. Sano, M. Pope, and H. Kallmann, “Electroluminescence and band gap in anthracene,” *J. Chem. Phys.*, vol. 43, no. 8, pp. 2920–2921, 1965.

[19] C. W. Tang and S. A. Vanslyke, “Organic electroluminescent diodes,” *Appl. Phys. Lett.*, vol. 51, no. 12, pp. 913–915, 1987.

[20] B. J. Griiner, P. J. Hamer, R. H. Friend, H. Huber, U. Schera, and A. B. Holmes, “A High Efficiency Blue-Light-Emitting Diode Based on Novel Ladder Poly(p-phenylene)s,” no. 10, pp. 748–752, 1994.

[21] C. W. Tang, “Two-layer organic photovoltaic cell,” *Appl. Phys. Lett.*, vol. 48, no. 2, pp. 183–185, 1986.

[22] L. Meng, “Organic and solution-processed tandem solar cells with 17.3% efficiency,” *Science (80-.).*, vol. 361, no. 6407, pp. 1–10, 2018.

[23] A. J. Heeger, “25th anniversary article: Bulk heterojunction solar cells: Understanding the mechanism of operation,” *Adv. Mater.*, vol. 26, no. 1, pp. 10–28, 2014.

[24] T. Stübinger and W. Brütting, “Exciton diffusion and optical interference in organic donor-acceptor photovoltaic cells,” *J. Appl. Phys.*, vol. 90, no. 7, pp. 3632–3641, 2001.

[25] B. A. Gregg and M. C. Hanna, “Comparing organic to inorganic photovoltaic cells: Theory, experiment, and simulation,” *J. Appl. Phys.*, vol. 93, no. 6, pp. 3605–3614, 2003.

[26] Z. A. Lan, G. Zhang, X. Chen, Y. Zhang, K. A. I. Zhang, and X. Wang, “Reducing the Exciton Binding Energy of Donor–Acceptor-Based Conjugated Polymers to Promote Charge-Induced Reactions,” *Angew. Chemie - Int. Ed.*,

pp. 10236–10240, 2019.

[27] K. L. Shaklee and R. E. Nahory, “Valley-Orbit Splitting of Free Excitons? the Absorption Edge of Si,” *Phys. Rev. Lett.*, vol. 24, no. 17, pp. 942–945, 1970.

[28] F. Wudl, N. Sariciftci, L. Smilowitz, and A. . Heeger, “Photoinduced Electron Transfer from a Conducting Polymer to Buckminsterfullerene,” *Science (80-.).*, vol. 258, no. 5087, pp. 1474–1476, 1992.

[29] Y. Tamai, H. Ohkita, H. Benten, and S. Ito, “Exciton Diffusion in Conjugated Polymers: From Fundamental Understanding to Improvement in Photovoltaic Conversion Efficiency,” *J. Phys. Chem. Lett.*, vol. 6, no. 17, pp. 3417–3428, 2015.

[30] A. J. H. G. Yu,* J. Gao, J. C. Hummelen, F. Wudi, “Polymer Photovoltaic Cells: Enhanced Efficiencies via a Network of Internal Donor-Acceptor Heterojunctions,” *Science (80-.).*, vol. 270, pp. 1–3, 1995.

[31] A. Yazmaciyan, M. Stolterfoht, P. L. Burn, Q. Lin, P. Meredith, and A. Armin, “Recombination Losses Above and Below the Transport Percolation Threshold in Bulk Heterojunction Organic Solar Cells,” *Adv. Energy Mater.*, vol. 8, no. 18, pp. 1–8, 2018.

[32] G. J. Hedley, A. J. Ward, A. Alekseev, C. T. Howells, E. R. Martins, L. A. Serrano, G. Cooke, A. Ruseckas, and I. D. W. Samuel, “Determining the optimum morphology in high-performance polymer-fullerene organic photovoltaic cells,” *Nat. Commun.*, vol. 4, pp. 1–10, 2013.

[33] M. Nikolka, K. Broch, J. Armitage, D. Hanifi, P. J. Nowack, D. Venkateshvaran, A. Sadhanala, J. Saska, M. Mascal, S. H. Jung, J. K. Lee, I. McCulloch, A. Salleo, and H. Sirringhaus, “High-mobility, trap-free charge transport in conjugated polymer diodes,” *Nat. Commun.*, vol. 10, no. 1, pp. 1–9, 2019.

[34] S. A. Jenekhe, L. Lu, and M. M. Alam, “New conjugated polymers with donor-acceptor architectures: Synthesis and photophysics of carbazole-quinoline and phenothiazine-quinoline copolymers and oligomers exhibiting large intramolecular charge transfer,” *Macromolecules*, vol. 34, no. 21, pp. 7315–7324, 2001.

[35] G. H. L. Heintges, P. J. Leenaers, and R. A. J. Janssen, “The effect of side-chain substitution and hot processing on diketopyrrolopyrrole-based polymers for organic solar cells,” *J. Mater. Chem. A*, vol. 5, no. 26, pp. 13748–13756, 2017.

[36] I. Kang, H. J. Yun, D. S. Chung, S. K. Kwon, and Y. H. Kim, “Record high hole mobility in polymer semiconductors via side-chain engineering,” *J. Am. Chem. Soc.*, vol. 135, no. 40, pp. 14896–14899, 2013.

[37] A. Laventure and G. C. Welch, “A tetrachlorinated molecular non-fullerene acceptor for high performance near-IR absorbing organic solar cells †,” *J. Mater. Chem. C*, no. 6, pp. 9060–9064, 2018.

[38] G. Oklem, X. Song, L. Toppare, D. Baran, and G. Gunbas, “A new NIR absorbing DPP-based polymer for thick organic solar cells,” *J. Mater. Chem. C*, vol. 6, no. 12, pp. 2891–3106, 2018.

[39] B. G. Kim, X. Ma, C. Chen, Y. Ie, E. W. Coir, H. Hashemi, Y. Aso, P. F. Green, J. Kieffer, and J. Kim, “Energy level modulation of HOMO, LUMO, and band-gap in conjugated polymers for organic photovoltaic applications,” *Adv. Funct. Mater.*, vol. 23, no. 4, pp. 439–445, 2013.

[40] W. Li, K. H. Hendriks, A. Furlan, W. S. C. Roulofs, S. C. J. Meskers, M. M. Wienk and R. A. J. Janssen, “Effect of the fibrillar microstructure on the efficiency of high molecular weight diketopyrrolopyrrole-based polymer solar cells,” *Adv. Mater.*, vol. 26, no. 10, pp. 1565–1570, 2014.

[41] C. Z. Li, H. L. Yip, and A. K. Y. Jen, “Functional fullerenes for organic photovoltaics,” *J. Mater. Chem.*, vol. 22, no. 10, pp. 4161–4177, 2012.

[42] Z. Li, H. C. Wong, Z. Huang, H. Zhong, C. H. Tan, W. C. Tsoi, J. S. Kim, J. R. Durrant, and J. T. Cabral, “Performance enhancement of fullerene-based solar cells by light processing,” *Nat. Commun.*, vol. 4, pp. 1–7, 2013.

[43] B. Wang, Y. Fu, C. Yan, R. Zhang, Q. Yang, Y. Han, and Z. Xie, “Insight into the role of PC71BM on enhancing the photovoltaic performance of ternary organic solar cells,” *Front. Chem.*, vol. 6, no. JUN, pp. 1–8, 2018.

[44] C. B. Nielsen, S. Holliday, H. Y. Chen, S. J. Cryer, and I. McCulloch, “Non-Fullerene Electron Acceptors for Use in Organic Solar Cells,” *Acc. Chem. Res.*, vol. 48, no. 11, pp. 2803–2812, 2015.

[45] A. Foertig, J. Kniepert, M. Gluecker, T. Brenner, V. Dyakonov, D. Neher, and C. Deibel, “Nongeminate and geminate recombination in PTB7:PCBM Solar Cells,” *Adv. Funct. Mater.*, vol. 24, no. 9, pp. 1306–1311, 2014.

[46] H. Hoppe and N. S. Sariciftci, “Morphology of polymer/fullerene bulk heterojunction solar cells,” *J. Mater. Chem.*, vol. 16, no. 1, pp. 45–61, 2006.

[47] V. D. Mihailetchi, L. J. A. Koster, P. W. M. Blom, C. Melzer, B. de Boer, J. K. J. van Duren, and R. A. J. Janssen, “Compositional dependence of the performance of poly(p-phenylene vinylene):Methanofullerene bulk-heterojunction solar cells,” *Adv. Funct. Mater.*, vol. 15, no. 5, pp. 795–801, 2005.

[48] P. Kovacik, H. E. Assender, and A. A. R. Watt, “Morphology control in co-evaporated bulk heterojunction solar cells,” *Sol. Energy Mater. Sol. Cells*, vol. 117, pp. 22–28, 2013.

[49] B. Y. Kadem, A. K. Hassan, and W. Cranton, “The effects of organic solvents and their co-solvents on the optical, structural, morphological of P3HT:PCBM organic solar cells,” *AIP Conf. Proc.*, vol. 1758, no. 2016, 2016.

[50] J. J. Van Franeker, M. Turbiez, W. Li, M. M. Wienk, and R. A. J. Janssen, “A real-time study of the benefits of co-solvents in polymer solar cell processing,” *Nat. Commun.*, vol. 6, pp. 1–8, 2015.

[51] W. Ma, C. Yang, X. Gong, K. Lee, and A. J. Heeger, “Thermally stable, efficient polymer solar cells with nanoscale control of the interpenetrating network morphology,” *Adv. Funct. Mater.*, vol. 15, no. 10, pp. 1617–1622, 2005.

[52] S. H. Kim, M. J. Misner, T. Xu, M. Kimura, and T. P. Russell, “Highly oriented and ordered arrays from block copolymers via solvent evaporation,” *Adv. Mater.*, vol. 16, no. 3, pp. 226–231, 2004.

[53] E. Palomares, “Benzothiadiazole Substituted Semiconductor Molecules for Organic Solar Cells: The E ff ect of the Solvent Annealing Over the Thin Film Hole Mobility Values,” *J. Phys. Chem. C*, vol. 122, pp. 13782–13789, 2018.

[54] S. Kwon, H. Kang, J. H. Lee, J. Lee, S. Hong, H. Kim, and K. Lee, “Effect of Processing Additives on Organic Photovoltaics: Recent Progress and Future Prospects,” *Adv. Energy Mater.*, vol. 7, no. 10, 2017.

[55] J. Zhao, S. Zhao, Z. Xu, B. Qiao, D. Huang, L. Zhao, Y. Li, Y. Zhu, and P. Wang, “Revealing the Effect of Additives with Different Solubility on the Morphology and the Donor Crystalline Structures of Organic Solar Cells,” *ACS Appl. Mater. Interfaces*, vol. 8, no. 28, pp. 18231–18237, 2016.

[56] G. Li, V. Shrotriya, Y. Yao, and Y. Yang, “Investigation of annealing effects and film thickness dependence of polymer solar cells based on poly(3-hexylthiophene),” *J. Appl. Phys.*, vol. 98, no. 4, pp. 1–5, 2005.

[57] C. Xu, M. Wright, N. K. Elumalai, M. A. Mahmud, V. R. Gonçales, M. B. Upama, and A. Uddin, “Optimization of conjugated polymer blend concentration for high performance organic solar cells,” *J. Mater. Sci. Mater. Electron.*, vol. 29, no. 19, pp. 16437–16445, 2018.

[58] R. Schlaf, H. Murata, and Z. H. Kafafi, “Work function measurements on indium tin oxide films,” *J. Electron Spectros. Relat. Phenomena*, vol. 120, no. 1–3, pp. 149–154, 2001.

[59] M. S. Farhan, E. Zalnezhad, A. R. Bushroa, and A. A. D. Sarhan, “Electrical and optical properties of indium-tin oxide (ITO) films by ion-assisted deposition (IAD) at room temperature,” *Int. J. Precis. Eng. Manuf.*, vol. 14, no. 8, pp. 1465–1469, 2013.

[60] C. Istanbulluoglu, S. Goker, G. Hizalan, S. O. Hacioglu, Y. A. Udum, E. D.

Yildiz, A. Cirpan, L. Toppare, “Synthesis of a benzotriazole bearing alternating copolymer for organic photovoltaic applications,” *New J. Chem.*, no. 39, pp. 6623–6630, 2015.

[61] S. Moon, S. Khadtare, M. Wong, S. H. Han, G. C. Bazan, and H. Choi, “Hole transport layer based on conjugated polyelectrolytes for polymer solar cells,” *J. Colloid Interface Sci.*, vol. 518, pp. 21–26, 2018.

[62] A. M. Nardes, M. Kemerink, M. M. de Kok, E. Vinken, K. Maturova, and R. A. J. Janssen, “Conductivity, work function, and environmental stability of PEDOT:PSS thin films treated with sorbitol,” *Org. Electron. physics, Mater. Appl.*, vol. 9, no. 5, pp. 727–734, 2008.

[63] D. C. Watters, J. Kingsley, H. Yi, T. Wang, A. Iraqi, and D. Lidzey, “Optimising the efficiency of carbazole co-polymer solar-cells by control over the metal cathode electrode,” *Org. Electron. physics, Mater. Appl.*, vol. 13, no. 8, pp. 1401–1408, 2012.

[64] T. H. Lai, S. W. Tsang, J. R. Manders, S. Chen, and F. So, “Properties of interlayer for organic photovoltaics,” *Mater. Today*, vol. 16, no. 11, pp. 424–432, 2013.

[65] S. R. Cowan, A. Roy, and A. J. Heeger, “Recombination in polymer-fullerene bulk heterojunction solar cells,” *Phys. Rev. B - Condens. Matter Mater. Phys.*, vol. 82, no. 24, pp. 1–10, 2010.

[66] C. Sae-Kung, B. F. Wright, T. M. Clarke, G. G. Wallace, and A. J. Mozer, “Effects of Interfacial Layers on the Open Circuit Voltage of Polymer/Fullerene Bulk Heterojunction Devices Studied by Charge Extraction Techniques,” *ACS Appl. Mater. Interfaces*, vol. 11, no. 23, pp. 21030–21041, 2019.

[67] N. K. Elumalai and A. Uddin, “Open circuit voltage of organic solar cells: An in-depth review,” *Energy Environ. Sci.*, vol. 9, no. 2, pp. 391–410, 2016.

[68] X. Liu, C. Zhang, C. Duan, M. Li, Z. Hu, and J. Wang, “Morphology Optimization via Side Chain Engineering Enables All- Polymer Solar Cells with Excellent Fill Factor and Stability,” *J. Am. Chem. Soc.*, no. 140, pp. 8934–8943, 2018.

[69] X. Li, T. Yan, H. Bin, G. Han, L. Xue, F. Liu, Y. Yi, Z. G. Zhang, T. P. Russell, and Y. Li, “Insertion of double bond π-bridges of A-D-A acceptors for high performance near-infrared polymer solar cells,” *J. Mater. Chem. A*, vol. 5, no. 43, pp. 22588–22597, 2017.

[70] A. A. B. Alghamdi, D. C. Watters, H. Yi, S. Al-Faifi, M. S. Almeataq, D. Coles, J. Kingsley, D. G. Lidzey, and A. Iraqi, “Selenophene vs. thiophene in benzothiadiazole-based low energy gap donor–acceptor polymers for

photovoltaic applications," *J. Mater. Chem. A*, vol. 1, no. 16, p. 5165, 2013.

[71] J. J. Intemann, K. Yao, H. L. Yip, Y. X. Xu, Y. X. Li, P. W. Liang, F. Z. Dhing, and X. Li, "Molecular weight effect on the absorption, charge carrier mobility, and photovoltaic performance of an indacenodiselenophene-based ladder-type polymer," *Chem. Mater.*, vol. 25, no. 15, p. 3191, 2013.

[72] H. Chen, J. Hou, S. Zhang, Y. Liang, G. Yang, and Y. Yang, "Polymer solar cells with enhanced open-circuit voltage and efficiency," *Nat. Photonics*, vol. 3, p. 653, 2009.

[73] H. J. Son, W. Wang, T. Xu, Y. Liang, Y. Wu, G. Li, and L. Yu, "Synthesis of Fluorinated Polythienothiophene- co -benzodithiophenes and Effect of Fluorination on the Photovoltaic Properties," *J. Am. Chem. Soc.*, vol. 133, p. 1890, 2011.

[74] H. Zhou, L. Yang, A. C. Stuart, S. C. Price, S. Liu, and W. You, "Development of Fluorinated Benzothiadiazole as a Structural Unit for a Polymer Solar Cell of 7 % Efficiency **," *Angew. Chem., Int. Ed.*, vol. 50, p. 2995, 2011.

[75] D. Keles, M. C. Erer, E. Bolayir, S. C. Cevher, G. Hizalan, L. Toppare, and A. Cirpan, "Conjugated polymers with benzothiadiazole and benzotriazole moieties for polymer solar cells," *Renew. Energy*, vol. 139, pp. 1184–1193, 2019.

[76] P. Deng, L. Liu, S. Ren, H. Li, and Q. Zhang, "N-acylation: An effective method for reducing the LUMO energy levels of conjugated polymers containing five-membered lactam units," *Chem. Commun.*, vol. 48, no. 55, pp. 6960–6962, 2012.

[77] Y. Llif, M. S. Liu, and A. K. Jen, "Synthesis and characterization of a novel and highly efficient light-emitting polymer," *Acta Polym.*, vol. 50, no. 2–3, pp. 105–108, 1999.

[78] A. Patra and M. Bendikow, "Polyselenophenes," *J. Mater. Chem.*, vol. 20, no. 3, p. 423, 2010.

[79] H.-Y. Chen, S.-C. Yeh, C.-T. Chen, and C.-T. Chen, "Comparison of thiophene- and selenophene-bridged donor–acceptor low bandgap copolymers used in bulk-heterojunction organic photovoltaics †," *J. Mater. Chem.*, vol. 22, p. 21552, 2012.

[80] B. Kim, H. R. Yeom, M. H. Yun, J. Y. Kim, and C. Yang, "A Selenophene Analogue of PCDTBT: Selective Fine-Tuning of LUMO to Lower of the Bandgap for E ffi cient Polymer Solar Cells," *Macromolecules*, vol. 45, p. 8660, 2012.

[81] M. Yuan, P. Yang, M. M. Durban, and C. K. Luscombe, "Low Bandgap

Polymers Based on Silafluorene Containing Multifused Heptacylic Arenes for Photovoltaic Applications," *Macromolecules*, vol. 45, no. 15, p. 5935, 2012.

[82] T.-Q. Nguyen, I. B. Martini, J. Liu, and B. J. Schwartz, "Controlling Interchain Interactions in Conjugated Polymers: The Effects of Chain Morphology on Exciton−Exciton Annihilation and Aggregation in MEH−PPV Films," *J. Phys. Chem. B*, vol. 104, no. 2, pp. 237–255, 2000.

[83] G. Hızalan, A. Balan, D. Baran, and L. Toppare, "Spray processable ambipolar benzotriazole bearing electrochromic polymers with multi-colored and transmissive states," *J. Mater. Chem.*, vol. 21, no. 6, pp. 1804–1809, 2011.

[84] V. Cuesta, M. Vartanian, P. Malhotra, S. Biswas, P. de la Cruz, G. D. Sharma, and F. Langa, "Increase in efficiency on using selenophene instead of thiophene in π-bridges for D-π-DPP-π-D organic solar cells," *J. Mater. Chem. A*, vol. 7, no. 19, pp. 11886–11894, 2019.

[85] S. W. Cho, L. J. F. Piper, A. DeMasi, A. R. H. Preston, K. E. Smith, K. V. Chauhan, P. Sullivan, R. A. Hatton, and T. S. Jones, "Electronic Structure of C60/Phthalocyanine/ITO Interfaces Studied using Soft X-ray Spectroscopies," *J. Phys. Chem. Cna*, no. 114, pp. 1928–1933, 2010.

[86] M. Akbayrak and A. M. Önal, "Synthesis and electrochemical polymerization of diketopyrrolopyrrole based donor–acceptor–donor monomers containing 3,6- and 2,7-linked carbazoles," *Polym. Chem.*, vol. 7, no. 39, p. 6115, 2016.

[87] N. A. Unlu, T. K. Deniz, M. Sendur, and A. Cirpan, "Effect of dithienopyrrole unit on electrochromic and optical properties of benzotriazole-based conjugated polymers," *Macromol. Chem. Phys.*, vol. 213, no. 18, p. 1890, 2012.

[88] W. Li, K. H. Hendriks, W. S. C. Roelofs, Y. Kim, M. M. Wienk, and R. A. J. Janssen, "Efficient Small Bandgap Polymer Solar Cells with High Fill Factors for 300 nm Thick Films," *Adv. Mater.*, vol. 25, no. 23, pp. 3182–3186, 2013.

[89] V. Vohra, K. Kawashima, T. Kakara, T. Koganezawa, I. Osaka, K. Takimiya, and H. Murata, "Efficient inverted polymer solar cells employing favourable molecular orientation," *Nat. Photonics*, vol. 9, no. 6, pp. 403–408, 2015.

[90] A. Tournebize, A. Rivaton, H. Peisert, and T. Chassé, "The crucial role of confined residual additives on the photostability of P3HT:PCBM active layers," *J. Phys. Chem. C*, vol. 119, no. 17, pp. 9142–9148, 2015.

[91] C. Li, X. Sun, J. Ni, L. Huang, R. Xu, Z. Li, H. Cai, J. Li, Y. Zhang, and J. Zhang "Methanol solvent treatment: A simple strategy to significantly boost efficiency and stability of air-processed ternary organic solar cells based on PTB7-Th:PCDTBT:PC70BM," *Org. Electron. physics, Mater. Appl.*, vol. 50,

pp. 63–69, 2017.

APPENDICES

A. Polymers Without Incorporation of π-bridges Investigated by Keleş et al.

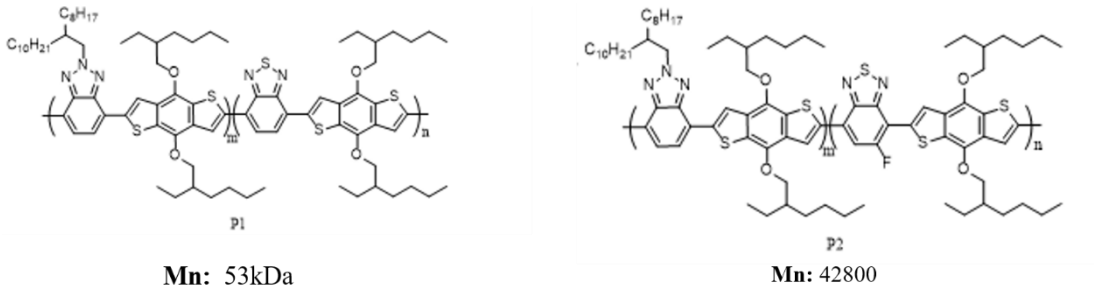

Mn: 53kDa
Mw: 124kDa

Mn: 42800
Mw:112000

Figure A.1. Structures of the polymers without polymer incorporation of π-bridges and their number average molecular weight (Mn) and weight average molecular weight (Mw) values

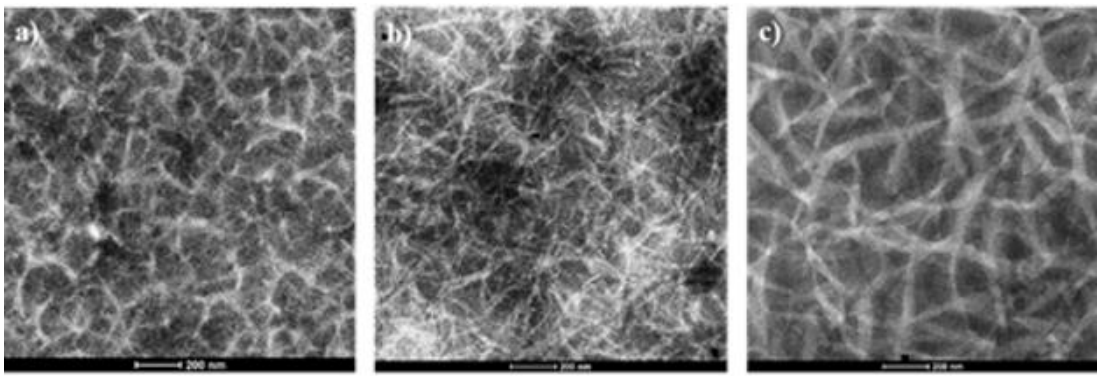

Figure A.2. TEM images of **a) P1**:$PC_{71}BM$ processed from o-dcb **b) P1**:$PC_{71}BM$ processed from o-DCB with 3% DIO, **c) P2**:$PC_{71}BM$ processed from o-DCB

As depicted in Figure A.2., although polymers P1 and P2 do not contain π-bridges in the polymer backbone, the due to the formation of narrower fibrils as they are relatively high molecular weight polymers, exciton diffusion to the donor acceptor interphase is driven. Hence, PCE values were measured as 4.10% and 3.84% respectively. Higher PCE value that non-fluorinated derivative P1 possess can be

contributed to the narrower fibril formation upon 3% DIO addition, which did not improve the morphology of fluorinated P2 [75].